

The effect of clouds and precipitation on the aerosol concentrations and composition in a boreal forest environment

Sini Isokääntä¹, Paul Kim², Santtu Mikkonen^{1,3}, Thomas Kühn^{1,4,*}, Harri Kokkola⁴, Taina Yli-Juuti¹, Liine Heikkinen^{5,6}, Krista Luoma⁵, Tuukka Petäjä⁵, Zak Kipling⁷, Daniel Partridge² and Annele Virtanen¹

5

¹Department of Applied Physics, University of Eastern Finland, Kuopio, 70210, Finland

²College for Engineering, Mathematics, and Physical Science, University of Exeter, Exeter, EX4 4QF, United Kingdom

³Department of Environmental and Biological Sciences, University of Eastern Finland, Kuopio, 70210, Finland

⁴Atmospheric Research Centre of Eastern Finland, Finnish Meteorological Institute, Kuopio, 70211, Finland

10 ⁵Institute for Atmospheric and Earth System Research (INAR) / Physics, Faculty of Science, University of Helsinki, Helsinki, 00014, Finland

⁶Department of Environmental Science (ACES) and Bolin Centre for Climate Research, Stockholm University, Stockholm, 10691, Sweden.

⁷European Centre for Medium-Range Weather Forecasts, Reading, RG2 9AX, United Kingdom

15

* now at: Weather and Climate Change Research, Finnish Meteorological Institute, Helsinki, 00101, Finland

Correspondence to: Sini Isokääntä (sini.isokaanta@uef.fi) and Annele Virtanen (annele.virtanen@uef.fi)

Abstract

20 Atmospheric aerosol particle concentrations are strongly affected by various wet processes, including ~~wet scavenging~~ (below and in-cloud ~~wet scavenging~~) and ~~in-cloud~~ aqueous phase oxidation ~~in-cloud~~. ~~This study employs air mass history analysis and observational data to investigate~~ We studied how wet scavenging and cloud processes affect particle concentrations and composition during transport to a rural boreal forest site in northern Europe. ~~For this investigation, we employed air mass history analysis and observational data.~~ Long-term particle ~~number~~ size distribution (~ 15 years) and composition measurements (~ 8 years) were ~~utilized in combination~~ combined with air mass trajectories with relevant variables (~~e.g. rainfall rate, relative humidity, mixing layer height~~) from reanalysis data. ~~Some such variables were rainfall rate, relative humidity, and mixing layer height.~~ Additional observational data-sets (~~e.g. such as~~ temperature ~~and~~; trace gases,) ~~were used to help~~ further evaluate ~~the~~ wet processes along trajectories with mixed effects models.

All ~~investigated~~ chemical species ~~investigated~~ (sulfate, black carbon and organics) ~~showed an exponentially~~ decreased ~~in the~~ particle mass concentration as a function ~~of~~ accumulated precipitation along the air mass route. ~~Clear seasonal differences in~~

30 ~~wet removal were observed for~~ In sulfate (SO₄) aerosols, clear seasonal differences in wet removal emerged, whereas organics (Org) and black carbon (eBC) ~~showed more~~ exhibited only minor differences. The removal efficiency varied slightly among the different reanalysis datasets (ERA-Interim and GDAS) used for the trajectory calculations, due to the difference in the average occurrence of precipitation events along the air mass trajectories between the reanalysis datasets. Aqueous phase processes were investigated by using a proxy for air masses travelling inside clouds. We compared air masses

35 with no experience of approximated in-cloud conditions or precipitation during the past 24 hours to air masses recently inside non-precipitating clouds, before they entered SMEAR II. Significant increases in ~~total~~ SO₄ mass concentration were observed ~~for for the latter air masses (recently experienced non-precipitating clouds), air masses recently been inside non-precipitating clouds when compared to air masses that had no experience of clouds or precipitation during the last 24 hours before arrival to SMEAR II.~~

40 Our Mmixed effects model considered, in which other contributing factors affecting particle mass concentrations in SMEAR II; examples were (e.g. trace gases, local meteorology, and, diurnal variation,) affecting particle mass concentrations in SMEAR II were considered, This model also indicated in-cloud SO₄ production ~~of SO₄~~. Despite the reanalysis dataset used in the trajectory calculations, aqueous phase SO₄ formation ~~of SO₄~~ was observed ~~despite the reanalysis dataset used in the trajectory calculations.~~ Investigation of the Pparticle number size distribution measurements revealed that most of the in-

45 cloud SO₄ formed ~~in cloud~~ can be attributed to particle sizes larger than 200 nm (electrical mobility diameter). ~~No significant formation of a~~queous phase secondary organic aerosol (aqSOA) formation was ~~observed~~ non-significant.

1 Introduction

Atmospheric aerosol particle concentrations are governed by their sources and sinks. Scavenging of aerosol particles by cloud droplets, ice crystals and precipitation i.e. wet scavenging, is one of the most essential aerosol particle removal processes in the atmosphere. Therefore, a detailed understanding of wet scavenging is necessary e.g. for atmospheric models to better simulate particle number size distribution, aerosol burden and long-range transport, especially to remote (e.g. arctic) areas. Aerosol wet scavenging can be distinguished into in-cloud scavenging, where the particles activate to cloud droplets or ice crystals (nucleation scavenging) which can further collide with interstitial aerosol (impaction scavenging) and are then removed by precipitation, and below-cloud scavenging, where aerosol particles are collected through collisions with falling raindrops and removed from the air (e.g. Ohata et al., 2016). Below-cloud scavenging is an efficient removal process for ultrafine and coarse particles, whereas in-cloud scavenging is the most important sink for accumulation mode particles (e.g. Andronache, 2003; Textor et al., 2006; Croft et al., 2009; Ohata et al., 2016).

The below-cloud scavenging rate is affected by the rainfall intensity as well as the collection efficiency which is controlled by both the particle and droplet size (e.g. Leong et al., 1983; Andronache, 2003; Chate et al., 2003) as well as the type of precipitation (Andronache et al., 2006; Paramonov et al., 2011). The below-cloud collection efficiency is the fraction of collected particles of diameter d_p contained within a collision volume of a drop having diameter D_p . The collision between aerosol particles and rain droplet is defined by Brownian diffusion, interception and impaction processes (e.g. Bae et al., 2012). The efficiency of below-cloud wet scavenging is often described by the scavenging coefficient. It is defined as the fraction of aerosol particles captured by raindrops per unit of time and is typically calculated from ambient observations before and after a precipitation event. A number of studies have determined aerosol scavenging coefficients for various particle sizes under various rainfall rates (e.g. Nicholson et al., 1991; Andronache, 2003; Laakso et al., 2003; Blanco-Alegre et al., 2018).

The in-cloud scavenging efficiency is controlled by nucleation (i.e. aerosol activation) and impaction scavenging. It is dominated by activation of aerosol particles into cloud droplets (e.g. Ohata et al., 2016), from which a fraction precipitate. Hence, it depends strongly on the updraft velocities at cloud base which along with the properties of the aerosol size distribution and the growing cloud droplet population governs the supersaturation conditions realised close to cloud base (Dusek et al., 2006; Partridge et al., 2012). If supersaturation conditions are well constrained from in-situ observations, the process of particles activating into cloud droplets can be relatively well described by current droplet activation parameterisations (e.g. Abdul-Razzak and Ghan, 2000; Nenes and Seinfeld, 2003; Fountoukis and Nenes, 2005) especially for a basic inorganic chemical species, e.g. sea salt. However, still large uncertainties exist regarding the role of chemical composition in droplet formation (e.g. Lowe et al., 2019), and further constraining is needed as particle chemical composition is also one of the key factors in droplet formation (Duplissy et al., 2011; Wu et al., 2013; Pajunoja et al., 2015; Väisänen et al., 2016). After the activation, impaction scavenging between the interstitial particles and cloud droplets is also occurring within clouds but it influences sub-micrometer particle concentrations relatively little (Croft et al., 2010).

80 ~~Scavenging of aerosol particles is not only affecting their number, but also their mass and other microphysical properties can change. Aerosol particles are not only scavenged by clouds but also their mass and properties can change due to aqueous phase processes.~~ Sulfate production caused by aqueous phase oxidation of gaseous sulfur dioxide which condenses onto particles (e.g. Barth et al., 2000; Ervens, 2015) is considered to be one of the most important mass addition pathways inside clouds (e.g. Harris et al., 2014; Ervens, 2015 and references therein). It has been estimated that in-cloud oxidation of sulfur
85 might contribute significantly (~60–90 %) to the global sulfate budget (Ervens, 2015). The production of secondary organic aerosol through aqueous phase processes (aqSOA) has been also reported (e.g. Ervens et al., 2011; El-Sayed et al., 2015; Ervens et al., 2018; Mandariya et al., 2019; Lamkaddam et al., 2021), ~~and~~ ~~it~~ has been suggested that aqSOA formation is comparable in magnitude with SOA formation through gas phase oxidation processes (Ervens et al., 2011). The observations of in-cloud (or fog) formation of new aerosol mass exist (e.g. Sorooshian et al., 2006; Sorooshian et al., 2007; Wonaschuetz
90 et al., 2012; Xie et al., 2015; Gilardoni et al., 2016; Xue et al., 2016) but they are scarce especially in areas with relatively low pollution levels.

Few experimental studies have combined the information of chemical composition or hygroscopicity (i.e. ability of a particle to take up water) with both in-cloud and below-cloud wet scavenging to investigate if differences in composition cause variation in the wet scavenging efficiency of the particles. Chate et al. (2003) obtained the washout coefficients for heavy
95 rain for 0.02-10 μm particles having different chemical composition with a theoretical approach following the presentation given by Slinn (1983). In addition, Chate and Devara (2005), observed order of magnitude differences for the collision efficiencies between the particles and raindrops of various sizes for selected chemical compositions during thunderstorm and non-thunderstorm precipitation events. Wang et al. (2021) continued with the topic in a modelling study by investigating the effect of rainfall intensity and type for different aerosol species. They observed no differences in the wet scavenging
100 efficiency between different rainfall intensities for different aerosol species, but noted that higher rainfall intensities were needed for larger particles to acquire the same removal efficiency over the tropics. Xu et al. (2020) included air mass origins into their study of hygroscopicity and chemical composition of aerosols in Mace Head, on the coast of Ireland, and found out that wintertime aerosols were usually externally mixed for both continental and marine air masses.

The estimation of the scavenging coefficients is often Eulerian (see e.g. Zhang and Chen, 2007 for definitions of Eulerian and Lagrangian approaches), as e.g. in Wang et al. (2021), Chate and Devara (2005) and Chate et al. (2003), and based on the local precipitation measurements or modelled quantities. An Eulerian approach does not consider that the air masses arriving ~~at~~ the measurement site have most likely experienced rain during their transport history, thus altering the particle population during en-route. In addition, particle composition and number- and mass concentration may be highly dependent on the air mass source area. Alternatively, a Lagrangian approach has a key advantage ~~compared to~~ Eulerian
105 methodologies in that individual particle trajectories are employed to allow for a consideration of the effects of air mass history on the aerosol. Relatively few Lagrangian aerosol-precipitation history studies have been performed. Tunved et al. (2013) reported that air masses arriving from central Europe and Russia ~~at~~ the arctic measurement site (Zeppelin station,

Ny Ålesund, Norway) had a relatively high particle mass concentration in all seasons when compared to airmasses from other regions. They also investigated how precipitation during transport to Zeppelin influenced the local particle population and exhibited an exponential decrease in submicron particle mass as a function of accumulated precipitation along the airmass trajectories. They suggested that in-cloud scavenging, which is more efficient for larger particles, was the dominant removal process, and thus the largest particles, which have the largest mass, are first removed, followed by smaller particles. Kesti et al. (2020) investigated the effect of precipitation on the particle number size distribution along airmass trajectories as they travel over the Indian ocean to the Maldives. They observed that a greater reduction in the accumulation mode particle concentration usually coincided with precipitation along the trajectory. A recent study investigated how precipitation along airmasses affects aerosol mass and volume observed in Bermuda (Dadashazar et al., 2021). They concluded that remote marine boundary layer aerosol characteristics are relatively sensitive to the precipitation along the airmass trajectories. All these studies observed clear changes in the aerosol population (either mass or number concentration) due to the precipitation along the airmass route. Both Tunved et al. (2013) and Kesti et al. (2020) concluded that the particles in the accumulation mode size range show strongest sensitivity to the precipitation along the airmass trajectories. Dadashazar et al. (2021) observed strongest sensitivity of the $PM_{2.5}$ mass to accumulated precipitation of up to 5 mm, while accumulated precipitation exceeding this limit had only minor effects to the $PM_{2.5}$ mass. Similar behaviour was described by Tunved et al. (2013) – the particle number size distribution was clearly affected by up to 10 mm of accumulated precipitation and a horizontal asymptote was achieved beyond that.

To explore the influence of below-cloud scavenging during transport on observed aerosol size distribution and chemical composition in biogenically dominated environments, we utilize here nearly a 15-year long aerosol dataset from the boreal forest station, SMEAR II, including continuous particle number size distribution observations, and almost 8 years of particle composition measurements. These in-situ observations are combined with airmass trajectories calculated from the HYSPLIT trajectory model (Stein et al., 2015) driven by various reanalysis datasets to investigate how the local aerosol population is affected by various wet processes the aerosols experience during their route to SMEAR II. Our main objectives can be summarized into the following three research questions:

1. How efficiently are different chemical species removed from the atmosphere by precipitation?
2. How does the aqueous phase processing taking place in clouds alter the particle mass concentration and composition?
3. If in-cloud formation of new particle mass is observed, what is the size range this mass is distributed in?

140

2 Data and methods

2.1 Observations at SMEAR II, Hyytiälä, Finland

Our observational data includes long-term measurements of ~~various~~ aerosols, gases and meteorological variables collected in the SMEAR II (Station for Measuring Ecosystem–Atmosphere Relations: Hari and Kulmala, 2005) station in Hyytiälä, southern Finland. The majority of the data measured in SMEAR II is publicly available at an online database (Junninen et al., 2009, <https://smear.avaa.csc.fi/>). The station is classified as a rural measurement station surrounded by mostly homogeneous Scots pine (*Pinus Sylvestris*) forest as there are no significant pollution sources nearby. The closest larger city is Tampere which has 238,140 inhabitants (Statistics Finland, 2019), located ca. 50 km southwest from SMEAR II. The particle number size distributions were measured with a Differential Mobility Particle Sizer (e.g., Aalto et al., 2001), and our study covers the years from January 2005 to August 2019. The observations cover the size distribution between 3 and 1000 nm (electrical mobility equivalent particle diameter). Mass concentrations for the various size classes were calculated by assuming the particles were spherical and had a constant density of $\rho = 1.6 \text{ g cm}^{-3}$ (see e.g. Häkkinen et al., 2012). Sensitivity analysis was conducted with unit density, 1 g cm^{-3} , following the approach used in Tunved et al. (2013), but same conclusions could be drawn.

The chemical composition of the particulate matter at SMEAR II ~~was~~ were acquired with aethalometer (e.g. Drinovec et al., 2015) and Aerosol Chemical Speciation Monitor (ACSM: Ng et al., 2011). The equivalent black carbon (eBC, Petzold et al., 2013) mass concentration data were calculated for the time between July 2006 to August 2019 from aethalometer (AE31 for 2006 – 2017 and AE33 for 2018 – 2019) measurements, which provide absorption coefficients for various wavelengths. The eBC utilized here was derived from the absorption coefficient measured at $\lambda = 880 \text{ nm}$ (as e.g. in Singh et al., 2014; Helin et al., 2018).

AE31 data, that is not automatically corrected for filter loading effects like AE33 data, was corrected with the algorithm suggested by Virkkula et al. (2007). The cut-off diameter for the eBC measurements was $10 \mu\text{m}$. However, as most of the absorbing particulate matter at SMEAR II falls in the submicron range, the eBC measured for PM_{10} is only 10 % higher compared to PM_1 measurements (Luoma et al., 2019). Measurements from the ACSM instrument provided the bulk chemical composition of sub-micron particulate matter, being most efficient at measuring between $\sim 75\text{--}650 \text{ nm}$ (vacuum aerodynamic diameter), allowing particles up to $1 \mu\text{m}$ through with less efficient transmission (Liu et al., 2007). Previous studies, e.g. Chen et al. (2018) have highlighted that hygroscopic growth leads to a shift in the size of dry particles cut off by impactors during sampling. However, this issue is not relevant for these measurements as the cut size of the virtual impactor used at the inlet for ambient air was clearly larger ($2.5 \mu\text{m}$) than the upper limit of the ACSM measurement range, and after the virtual impactor, the aerosol was dried before entering the ACSM (Heikkinen et al., 2020). The data from the ACSM in this study extends from March 2012 to August 2019, including the mass concentrations ($\mu\text{g m}^{-3}$) of total organic (Org),

ammonium, (NH₄), sulfate (SO₄), nitrate (NO₃), and chloride (Chl). More details from the ACSM measurements and data treatment can be found from Heikkinen et al. (2020).

175 Other investigated gas phase variables included concentrations of gaseous nitrogen oxide (NO_x, in a unit of ppb), sulfur dioxide (SO₂, ppb), ozone (O₃, ppb) and carbon monoxide (CO, ppb). Variables describing the local meteorological conditions measured were air temperature (T , °C), atmospheric pressure at ground level (p , hPa), relative humidity (RH, %), precipitation (liquid water equivalent, rain_{local}, mm h⁻¹) solar radiation (SolR, W m⁻²), wind speed (WS, m s⁻¹) and wind direction (WD, °). Data coverage, summary statistics and list of the measurement instruments are shown in Tables S1-S3. All investigated variables are measured near ground level, below the tree canopy.

180 The original time resolution for each observational variable varies depending on the measurement instrument. Thus, each investigated variable was averaged into one hour means. All available observational data overlapping with the trajectories released every hour was investigated (January 2005-August 2019). Data points coinciding with reported wind direction between 120° and 140° were removed from the data set to exclude the influence from two nearby sawmills reported as major sources of VOCs and Org (e.g. Liao et al., 2011; Heikkinen et al., 2020). In addition, data rows for which the airmass back-
185 trajectory crossed the Kola peninsula (for the sake of data-analysis, we used a rectangular box with coordinates of 31-42° of longitude and 66-70° of latitude to estimate the geographical area of Kola Peninsula), were excluded from the analysis due to high pollution caused by industry in that area (e.g. Kulmala et al., 2000; Riuttanen et al., 2013; Heikkinen et al., 2020) as this strong SO₄ source could cause significant biases to our analysis. Further data-analysis was conducted in R Statistical Software and Python, and colour maps for the figures considering colour vision deficiencies were inspired by Crameri et al.
190 (2020).

2.2 Trajectory calculations and airmass source analysis

4-day (96 h) back trajectories were obtained using version 5.1.0 of the HYSPLIT (Hybrid Single-Particle Lagrangian Integrated Trajectory, Stein et al., 2015) model for the period from January 2005 to August 2019. 4-day long trajectories were selected, as that is typically long enough period so that even the slow moving airmasses have enough time to travel
195 from Atlantic and marine areas over to the boreal environment. The arrival height of the trajectories was set to 100 metres above ground level at the measurement station in SMEAR II. ERA-Interim reanalysis meteorology at 1 degree resolution was used as the input for calculating the trajectories which were released every hour leading to 24 trajectories per day (128,520 in total). In addition, reanalysis dataset of GDAS (1 degree resolution, <https://www.ready.noaa.gov/archives.php>) was used to further validate our conclusions obtained with the trajectories based on ERA-Interim reanalysis data.

200 The observational data has been temporally collocated with the airmass trajectory release times. Any measured variable extending past August 2019 has not been used in this study even if available as ERA-Interim reanalysis meteorological input has been superseded with ERA5 after that. Variables provided by HYSPLIT along each trajectory are also used in this study (in addition to the airmass route coordinates), namely the height of the airmass, rainfall rate at the surface (used as a proxy

for the experienced precipitation by the airmass), relative humidity in the airmass and mixing layer height (MLH) for the
205 current horizontal location of the air mass. The MLH provided from HYSPLIT at SMEAR II was used to estimate the actual
MLH due to absence of local long-term measurements of MLH at the site. Precipitation events along the trajectory are
relatively evenly distributed along the 96 hours (Figure S1), having slightly lower occurrence 12-18 hours before the
airmasses reach SMEAR II. Locally measured (surface) precipitation values agree relatively well with the estimate from
HYSPLIT (Figure S2).

210 The relative humidity at the altitude of the airmasses was used as a proxy for in-cloud cases. We selected a limit of RH > 94
% (as in Tunved et al., 2004) for which we assume the airmass is inside a cloud or fog (we do not separate these cases). We
would like to note that even if the approximation for the in-cloud cases is not very accurate based on the RH values only, the
humidity in these cases is high enough for the particles to have taken up significant amounts of water. Strong hygroscopic
growth can be observed before activation, and e.g. for inorganic salts the deliquescence RH is well below 94 % (e.g. Cruz
215 and Pandis, 2000; Zieger et al., 2017; Lei et al., 2018). Thus, it is safe to assume the aqueous phase processes, whether in
cloud or inside fogs, are taking place when RH of 94 % is exceeded. The selected limit for the in-cloud cases is relatively
close to the values used for critical RH for cloud formation in reanalysis data and large-scale models. For example, in ERA-
Interim values between 80 % to 100 % with increasing values towards the surface are used (Tiedtke, 1993; Dee et al., 2011).
In MPI-ESM model (ECHAM6.3), the limit has been given values between 90 % to 96.8 % close to the surface (Mauritsen
220 et al., 2019). Sensitivity analysis was conducted with RH limits of 85 %, 90 % and 98 %, but same conclusions could be
drawn.

The air parcel trajectories we have obtained from HYSPLIT simulate the large-scale airmass transport. As trajectories are
derived from the reanalysis data with 1 degree resolution (~100 km x 100 km), they do not resolve any sub-grid scale
processes. Therefore, they will not capture transport through individual clouds, which could be in the order of hundreds of
225 meters. The airmass transport routes, and the clouds/precipitation in our study, can thus be tied to the average meteorological
properties of reanalysis grid box that the trajectories cross. In addition, since the precipitation data is not vertically resolved,
it is possible that the air parcel is above the precipitating cloud, and thus not affected by the precipitation. Other possible
scenario would be a case where our airmass is below the precipitating cloud, but precipitation evaporated before influencing
our air parcel. This is an unfortunate limitation in this type of analysis and may contribute to the variability of the results.
230 Despite, successful analyses have been conducted recently (Kesti et al., 2020; Dadashazar et al., 2021).

For the statistical model analysis used to support our findings, the airmass trajectories were clustered into source areas by
kmeans-clustering, in which the trajectories are partitioned into k clusters and for each cluster a centroid is defined (e.g.
Kaufman and Rousseeuw, 1990). Each trajectory is then allocated to the nearest cluster, providing us with geographical
source areas for the airmasses to be used as random effects in the mixed effects model (Section 2.3). Clustering was
235 performed using the R Statistical software with the help of the cluster-package (Maechler et al., 2019; R Core Team, 2019)
using the Hartigan-Wong algorithm (Hartigan and Wong, 1979). Other clustering techniques were tested (e.g. partitioning
around medoids with different distance metrics), but kmeans provided distinct enough clusters for our purposes. The

appropriate number of clusters was determined by evaluating the interpretability of the clusters and inspecting the total within sum of squares (WSS) for different number of clusters in which the “knee” of the WSS curve (indicating smallest dissimilarities within clusters) could indicate the number of clusters (3 to 6 in our case). The final clusters, i.e. source areas are show in Figures S3 and S4. The statistical model showed no strong sensitivity towards the number of clusters, i.e. same conclusions could be drawn with 4, 5 and 6 clusters.

2.3 Statistical mixed effects model

~~2.3.1 General description of the multivariate mixed effect model~~

Multivariate mixed effects models were used to investigate the significance of various processes affecting the particle concentrations at the SMEAR II site. Mixed effects models were used as they estimate the variance-covariance structure of the data in addition to the mean of the response variable, and are better justified for grouped data sets with possible hierarchical structures (as e.g. in this study, by airmass sources, months, hour of the day etc.) than fixed effect models (Mehtätalo and Lappi, 2020). In addition, statistical mixed effects models are an effective tool when interactions between variables are investigated (see e.g. Mikkonen et al., 2011). For example, a study from Yli-Juuti et al. (2021) used a linear mixed effects model to distinguish the direct/real effect of temperature from other variables affecting the concentration of organic aerosols when investigating the organic aerosol driven climate feedback in the same boreal area. Linear mixed effects model can be presented in general form as

$$\mathbf{y} = \mathbf{X}\boldsymbol{\beta} + \mathbf{Z}\mathbf{b} + \boldsymbol{\epsilon}, \quad (1)$$

where \mathbf{y} is the vector of the response variable, $\boldsymbol{\beta}$ and \mathbf{b} are the vectors of fixed and random effects, respectively and \mathbf{X} and \mathbf{Z} are the related design/coefficient matrices (McCulloch et al., 2008). Vector $\boldsymbol{\epsilon}$ includes the random errors. Depending on the structure of the random effects (crossed or nested effects), the relationship between \mathbf{X} and \mathbf{Z} varies (McCulloch et al., 2008). In our study, we also needed to consider the observed exponential dependency between the response variables and the accumulated precipitation (see Section 3.1) and thus we used a nonlinear mixed effects model. The nonlinear mixed effects models (separate model for each chemical species) were applied with R statistical software (R Core Team, 2019) with *nlmer*-function provided by the package lme4 (Bates et al., 2015). The formulation of the final fitted equation and the variables used in the regression are presented in Appendix A. Regression coefficients and more details on the variable selection are presented in the supplementary material in Section S3. The formulation of the final fitted equation is expressed as

$$[\text{VAR}]_t = \beta_0 + \{\mathbf{b}_h + \mathbf{b}_m + \mathbf{b}_y\} + \{\beta_1[\text{NO}_x]_t + \beta_2[\text{SO}_{2,t}] + \beta_3[\text{O}_3]_t + \beta_4[\text{CO}]_t\} + \{\beta_5 T_t + \beta_6[\text{MLH}]_t\} + \{\exp(\beta_7 \text{accum. precip.}_t) + \beta_8 \text{time. in. cloud}_t\} + \{\beta_9 \text{emission. col. time}_t + \beta_{10} \text{time. in. land}_t + \mathbf{b}_a\}, \quad (2)$$

where [VAR] is now the mass concentration of either Org, SO₄ or eBC, β_0 is a model intercept, \mathbf{b}_h , \mathbf{b}_m , \mathbf{b}_y and \mathbf{b}_a are the vectors of random intercepts for hour of the day, month, year and airmass source area, respectively, and $\beta_1 - \beta_{10}$ are the fixed

270 regression coefficients. Subscript i denotes the time point i.e. one observation. Thus the predictor variables (see Section 2.1 for the abbreviations) include concentrations of SO₂, CO, NO_x and O₃ (trace gases); air T and MLH (at SMEAR II derived from the back trajectory data) describing the local meteorology and following trajectory derived variables: accumulated precipitation along the trajectory (mm), time spent in high humidity conditions without simultaneous rain (“in non-precipitating cloud”, h), emission collection time (time in mixed layer until rain event, h) and total time the air mass has spent over land (h). In addition, the air mass source areas (obtained by clustering as explained in Section 2.2, visualised in Figures S3 and S4) and observation year, month and hour of the day were included, as shown in Eq. (2). Summary of the used
 275 predictor variables in the regression is shown in Table 1 and each predictor variable group is separated with curly brackets in Eq. (2). The process leading to the selection of the response variables is explained in the Section 2.3.2.

Table 1 Predictor variables used in regression.

Group	Name	Variables included
1	Base variability (diurnal, seasonal, random)	Observation year and month, hour of the day
2	Trace gases	NO _x , SO ₂ , O ₃ , CO
3	Local meteorology	T , MLH
4	Wet processing along the trajectory	Accumulated precipitation, time spent in non-precipitating cloud
4a	Wet scavenging	Accumulated precipitation
4b	In-cloud aqueous phase processing	Time spent in non-precipitating cloud
5	Long range transport	Air mass source area, emission collection time, time spent above land

280 2.3.2 Selection of relevant variables and determining the relative contribution of variable groups

In this section we justify our decision to leave out some of the variables, that could be considered relevant for the response variables (Org, eBC, SO₄) we investigated. Variables that were investigated but were excluded from the final model were RH, SolR, WS, WD, rain_{local} and p . RH has strong correlation coefficient (> 0.5) with MLH and having both in the model violates the assumption of the model on relatively independent predictors and causes collinearity issues on the computation
 285 (e.g. Dormann et al., 2013). When comparing models with either RH or MLH, the models with MLH had better predictive capability, thus MLH was selected. MLH also has high correlation coefficient SolR, but again the model with MLH had better predictive capability and thus SolR was discarded from further analysis. In addition, including both, RH and SolR, had negligible effect on goodness of fit indicators or did not change the other regression coefficients significantly indicating their presence in the model does not improve the overall fit. WS, WD, rain_{local} and p were not significant predictors for the

290 models based on a likelihood ratio test (Wilks, 1938) made between different model versions. Simultaneous observations of
the selected variables were used in the final regression, including 22,778 observations in total from the period between
March 2012 and August 2019. The division into two seasons based on monthly median temperature T_m (discussed in detail in
Section 3.1) led to 14,501 observations for warm months ($T_m > 10$ °C) and 8,277 observations for the cold months ($T_m < 10$
°C).

295 To investigate how strong and/or significant an effect each predictor group shown in Table 1 has for the observed variable
(Org, eBC, SO₄) relative to all other predictor groups, we applied Bayesian Information Criterion (BIC, Schwarz, 1978)
derived for each of the fitted models. BIC is a criterion which can be used in model selection as models with lower BIC are
preferred (Schwarz, 1978). It is based on likelihood function and includes a penalty term for the number of variables in a
model to avoid overfitting (Schwarz, 1978; Stoica and Selen, 2004). Each variable group was removed in turn from the full
300 model (separate models for each species) presented in Eq. (2), and the BIC for the reduced model was compared to the BIC
of the full model. With this approach, we were able to determine the relative contribution of each variable group for the
investigated species (response variable). Regression coefficients and relative contributions are reported in Section S3.

3 Results and discussion

3.1 Effect of wet scavenging on the aerosol concentrations

305 The evolution of the total aerosol mass (assuming unit density, $1 \mu\text{g m}^{-3}$) and number concentration derived from the DMPS size distribution as a function of accumulated precipitation along the air mass trajectories are shown in Figure 1. The hourly rainfall values at the surface (mm h^{-1}) provided by the HYSPLIT trajectory data were integrated over the 96-hour period for each trajectory to acquire the total accumulated precipitation during each trajectory at SMEAR II. The accumulated precipitation was then grouped into 0.5 mm bins, and for each bin median particle mass was calculated. Bins which had less

310 than 10 data points were discarded due to low statistics (and thus not shown in Figure 1). The sample size for each bin corresponding to Figure 1 is demonstrated in Figure S5. The particle mass derived from both DMPS and ACSM measurements (Figure S6, corresponding sample size in Figure S7) show exponential decrease (as a function of accumulated precipitation) similarly to the results reported by Tunved et al. (2013) for arctic aerosols. Particle mass decrease reaches asymptote after ~10 mm of accumulated precipitation. This could be due to local sources producing significant amounts of particles even though arrived air masses have experienced large amounts of precipitation during travel. Similar behaviour has been observed for Arctic location and in tropics (Tunved et al., 2013; Dadashazar et al., 2021). The total particle number (Figure 1b) also shows a decrease in the concentration, but not as clear exponential decrease as shown for the particle mass concentration. The behaviours of the particle mass and number as a function of accumulated precipitation do not depend on the choice of reanalysis data used to drive the HYSPLIT trajectory model (Figure S229).

320 It should be noted here that this type of approach to air mass history analysis in which the vertical trajectory position with respect to precipitating cloud is not considered, does not allow us to explicitly separate the in-cloud (particles activate to cloud droplets and collide with interstitial aerosol and then precipitate) and below-cloud (falling droplets collide with particles) precipitation scavenging (see Section 2.2). Instead, it gives us an estimate of the overall effect of precipitation on aerosol concentrations by using the surface precipitation provided by the air mass trajectories as a proxy for the precipitation experienced by each single particle trajectory. In addition, as we investigate aerosol scavenging in a Lagrangian framework (visualized in Figure 2) in which the temporal and spatial scales of the reanalysis data used in the trajectory calculations are much larger than dynamic cloud processes, we cannot directly probe sub-grid scale processes, e.g. in-cloud aerosol scavenging. Lagrangian analysis demonstrates in-cloud scavenging occurring via the removal of activated aerosol particles from the atmosphere due to precipitation scavenging. However, this is the case only if the trajectory of the air parcel coincides with the conditions we define as “precipitating cloud”. Accordingly, ~~the Lagrangian analysis demonstrates in-cloud scavenging occurring via the removal of activated aerosol particles from the atmosphere due to precipitation scavenging, only if the clouds precipitate while the air parcel is passing them. Therefore, w~~When we investigate how the size distribution changes with accumulated precipitation as demonstrated in Figure 3, some qualitative conclusions can, however, be drawn. The strong exponential decay of particle number size distribution is visible in sizes larger than 100 nm while the

330

335 changes in size range around 10-50 nm are small or negligible. This indicates that the large particles ($d_p > 100$ nm) are removed most efficiently with the first 10 mm of accumulated precipitation while smaller particles remain unaffected by any amount of accumulated precipitation. Hence, the in-cloud scavenging in our investigation is greatly dependent on the activation of aerosol particles to cloud droplets, which in turn is strongly dependent on the particle size. The number concentration of particles with diameter larger than 100 nm has been widely used as a proxy for aerosol able to activate to cloud droplets. This is also the size range where we see the largest decrease in number concentrations ([Figure 3, especially Fig. 3b](#)) as a function of accumulated precipitation. We can qualitatively explain the observed behaviour in [Figure 3](#) according to a simplistic view of the complex and highly dynamical process of activation. ~~Assuming relatively constant meteorological conditions over our trajectory transport region, we can describe the precipitation cycle followingly in which the available supersaturation varies temporally and spatially during the cloud precipitation cycle:~~ after the larger particles are removed through activation into cloud droplets, of which a subset will precipitate, the size of the smallest activated particles decreases ~~in the consecutive cloud cycle,~~ because of less competition for the available supersaturation. ~~On the other hand, the~~

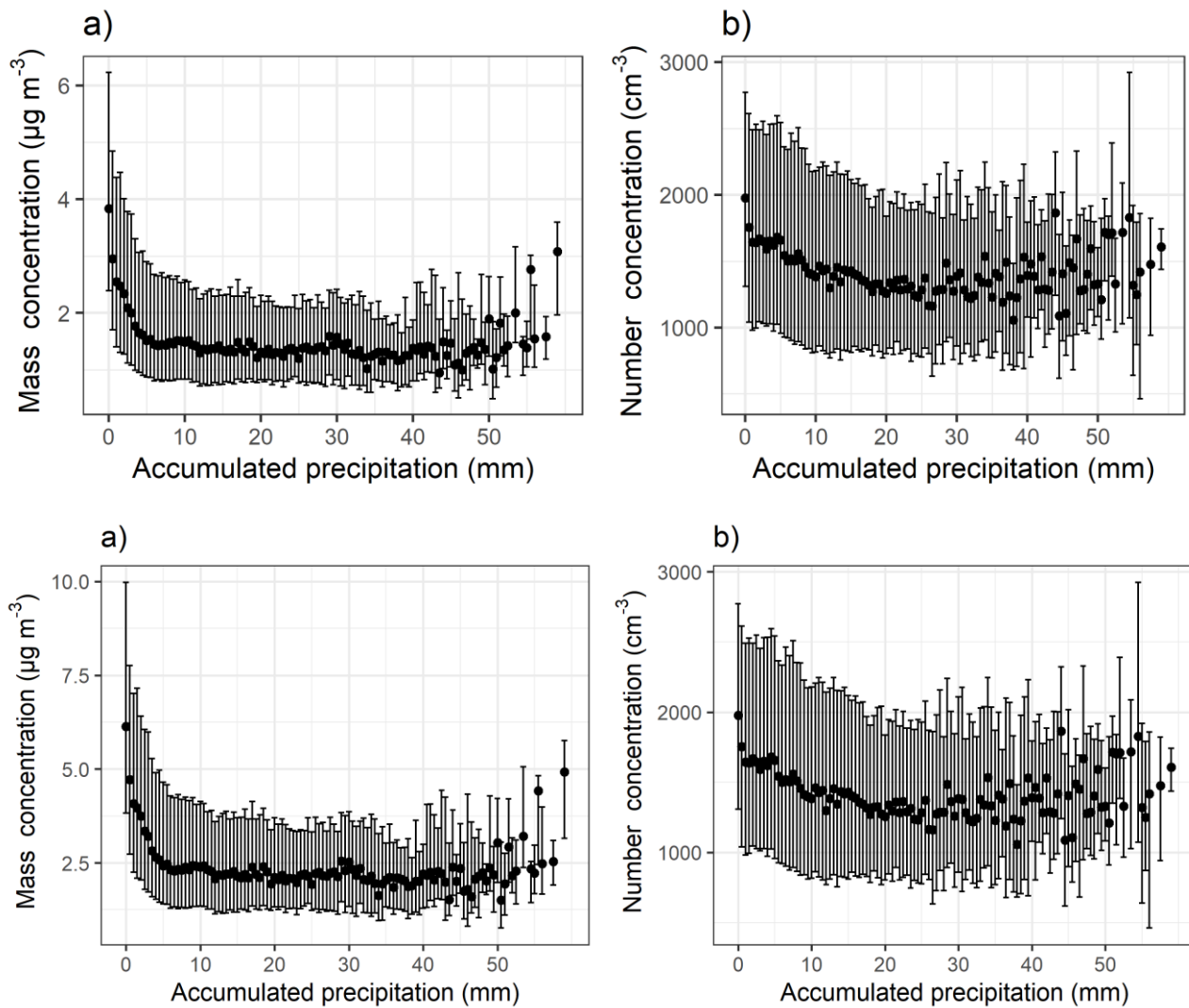
340 ~~The~~ lowest scavenging efficiency values for below-cloud scavenging are typically in the size range of some hundreds of nanometres ~~in diameter~~ depending on the precipitation type (e.g. Wang et al., 2010). ~~However, and~~ at size range below 100

345 nm, the scavenging efficiency increases strongly with decreasing particle size so that at 10 nm size range, it is significantly higher. Hence, if the below-cloud scavenging would play a major role at sub-micron size range considered here, we should see a decrease in the number concentration with accumulated precipitation in the smallest particle sizes where the below-cloud scavenging efficiencies are the highest. As shown in [Figure 3](#), the aerosol concentrations in size range of 10-50 nm show no ~~clear~~ sensitivity (~~decrease~~) to accumulated precipitation and the largest decrease in concentrations are shown in size

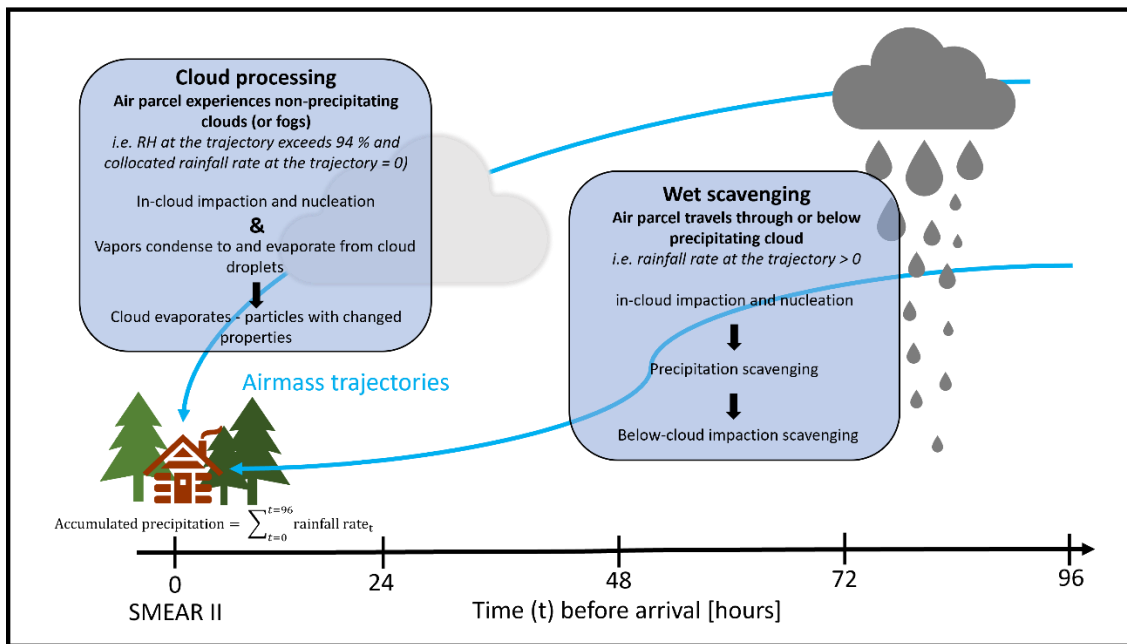
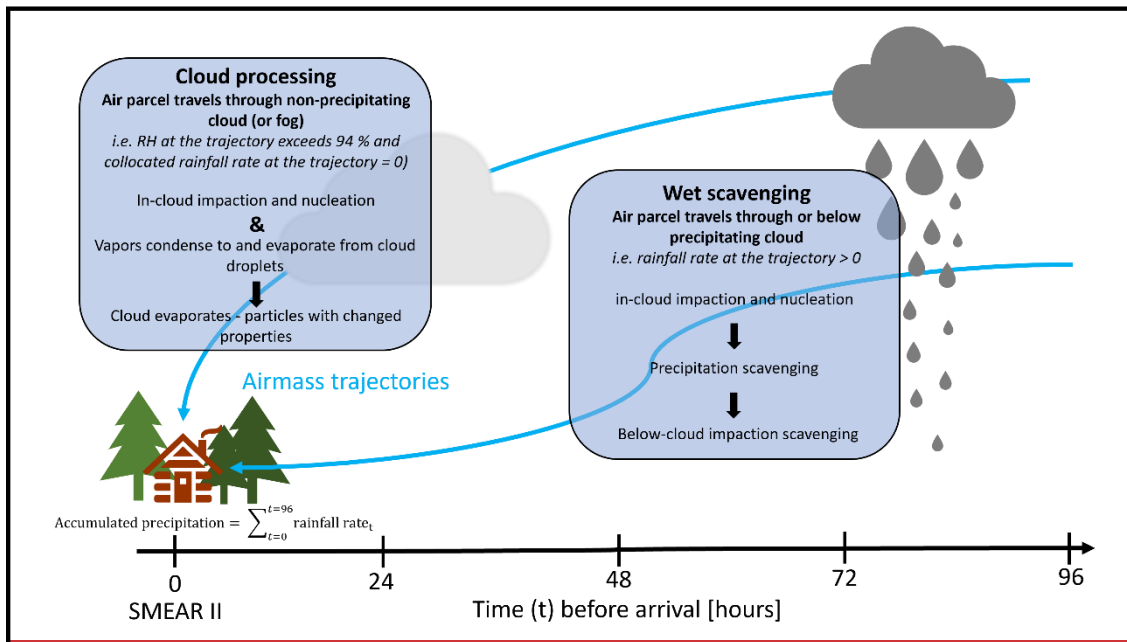
350 range of $d_p \gtrsim 100$ nm ~~and above~~ suggesting that ~~the~~ in-cloud scavenging is the dominating removal mechanism in the submicron particle size range in the studied environment. ~~Inspection of selected size ranges (Figure S8) confirms that only larger sizes start exhibiting the decrease as a function of the accumulated precipitation.~~ This has further support from earlier studies suggesting below-cloud scavenging to be a less important scavenging mechanism than in-cloud scavenging for accumulation mode sized particles (e.g. Tunved et al., 2013; Wang et al., 2021). Similar changes in the size distribution can

355 be observed when the analysis was repeated using GDAS reanalysis meteorology instead of ERA-Interim ([Figure S234](#)). Assuming now in-cloud scavenging to be dominating and referring back to [Figure 1](#), the difference in the decreasing trends between particle mass and number concentration arises likely from the fact that the aerosol mass is dominated by large ($d_p > 100$ nm) particles, which are more efficiently removed by in-cloud wet scavenging when compared to particles with smaller size. The aerosol number concentration, however, is dominated by particles with $d_p < 100$ nm which are not activated to

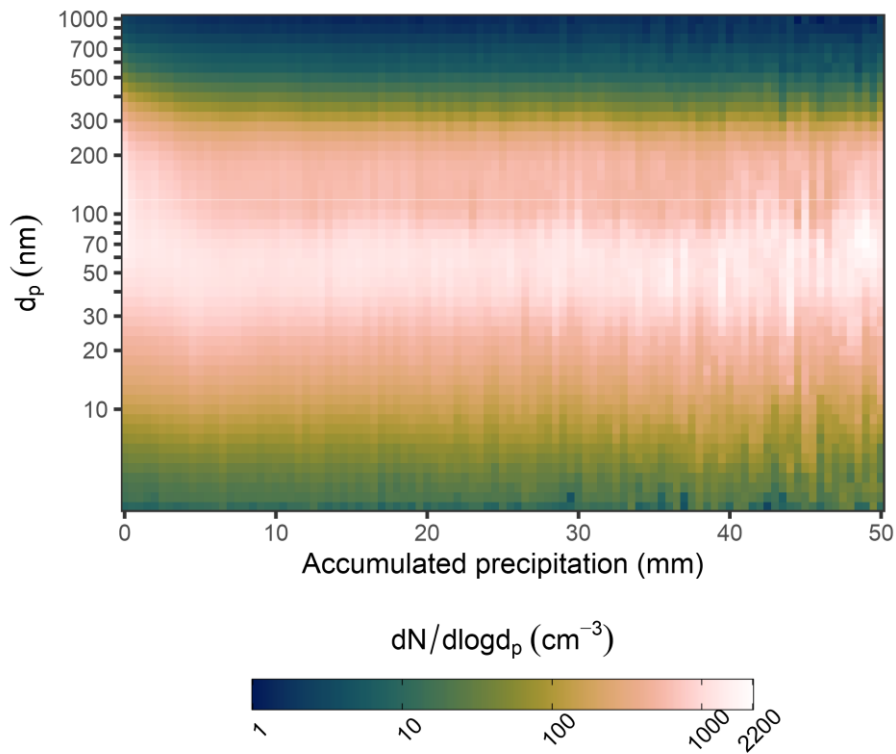
360 cloud droplets as efficiently as particles with larger size, and thus not removed when the cloud precipitates. Hence the in-cloud scavenging affects the removal much less when the total particle number is inspected than in the case of large particles dominating the mass loading.



370 **Figure 1** Total particle ($d_p = 3\text{-}1000$ nm) mass (a) and number (b) concentration as a function of 0-50 mm accumulated precipitation along the 96-hour HYSPLIT airmass trajectories. The black dots show the median values and bars highlight the 25th-75th percentiles for each 0.5 mm bin of accumulated precipitation. The figure includes DMPS data between January 2005 and August 2019.



375 **Figure 2** Schematic visualizing the wet processes along air mass trajectories in the Lagrangian framework. Travelling particles experience different conditions en-route thus alternating the observed particle concentrations (through scavenging) and composition (through cloud processing) at the SMEAR II.



380 **Figure 3** The aerosol size distribution ($d_p = 3\text{--}1000\text{ nm}$) as a function of the $0\text{--}50\text{ mm}$ of accumulated precipitation. Data is shown as medians for binned accumulated precipitation (bin size 0.5 mm). The figure includes DMPS data between January 2005 and August

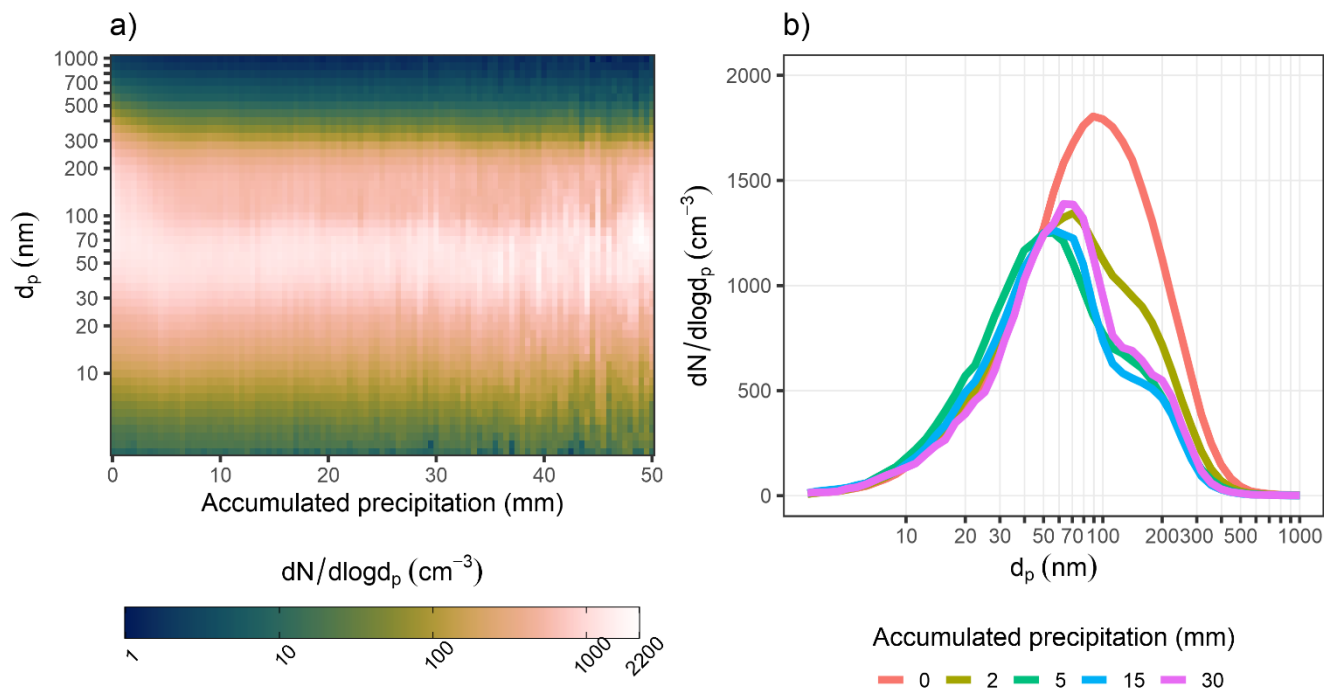


Figure 3 The aerosol size distribution ($d_p = 3\text{-}1000$ nm) as a function of the 0-50 mm of accumulated precipitation along 96-hour air mass trajectories is shown in a). Data is shown as medians for binned accumulated precipitation (bin size 0.5 mm). Median size distributions are presented for selected values of accumulated precipitation in b). Figure includes DMPS data between January 2005 and August 2019.

3.2 Effect of wet scavenging on the aerosol composition

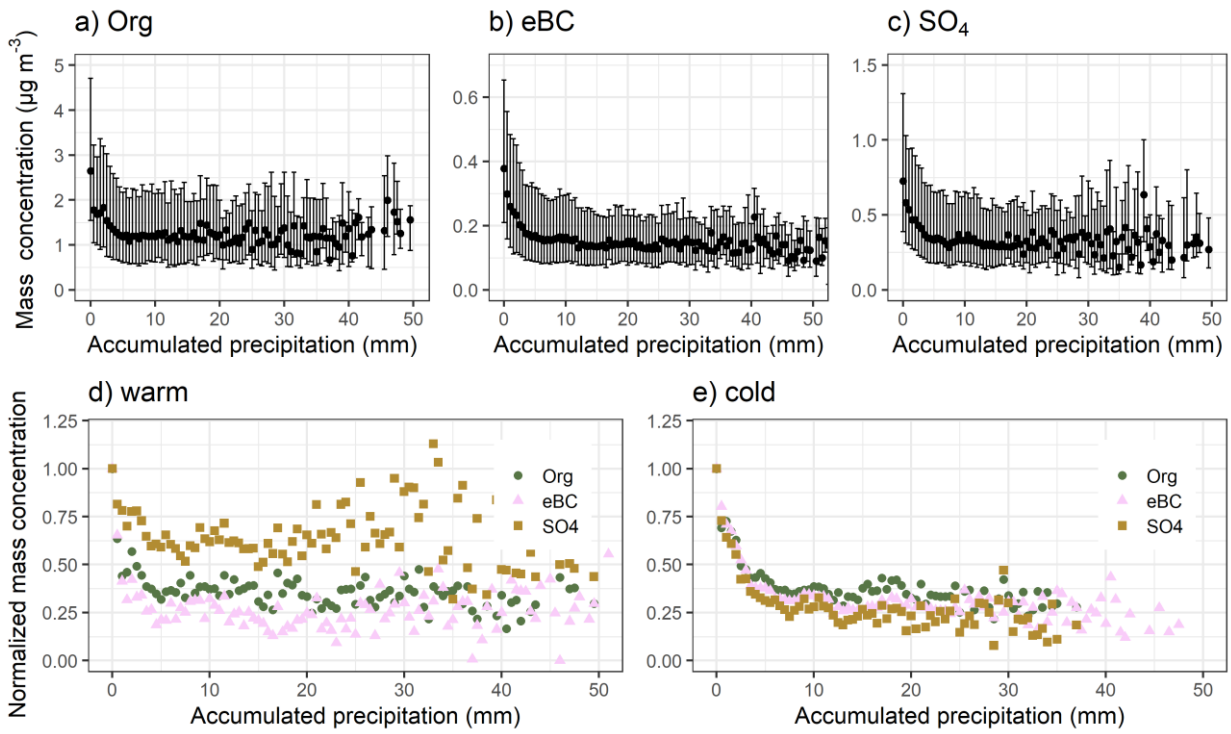
The effect of accumulated precipitation on the different chemical components (organics, sulfate, black carbon, nitrate, ammonium and chloride hereafter Org, SO_4 , eBC, NO_3 , NH_4 and Chl, respectively) can be investigated using the long-term observational data (see Section 2.1 for details). In this study, our focus is on SO_4 , Org and eBC and the other chemical species obtained with ACSM are included in the supplementary material as their mass concentrations are generally relatively low at SMEAR II (Heikkinen et al., 2020). To investigate possible seasonal differences in the wet scavenging of the particles, we divided the data based on monthly median temperatures (T_m). Months which have $T_m < 10$ °C (calculated from data between 2005-2019) include January, February, March, April, October, November, and December and hereafter referred as “cold” months. Months that have $T_m > 10$ °C include May, June, July, August, and September and are referred as “warm” months. This division into two seasons is used to ensure enough data points for each bin, as the chemical composition measurements are more limited than the particle number size distributions. Each of the studied chemical

components shows exponential decrease as a function of accumulated precipitation (Figure 4a-c), and similar decreases is also seen if the reanalysis data is changed (Figure S242a-c).

400 To investigate the possible differences in the removal efficiency for different species, we normalized the median mass concentration values with the median mass concentration value when the accumulated precipitation is zero (Figure 4d-e). The median mass concentrations (and 25th-75th percentiles) for non-precipitating trajectories for Org, eBC and SO₄ were 3.77 (2.18-5.49), 0.28 (0.17-0.45) and 0.52 (0.34-0.88) $\mu\text{g m}^{-3}$ for warm months and 2.03 (1.22-3.37), 0.48 (0.26-0.85) and 1.01 (0.51-1.53) $\mu\text{g m}^{-3}$ for cold months, respectively. Org mass concentration, for example, is much higher during warm months
405 due to strong local biogenic activity whereas SO₄ mass concentration in warm months is ~50 % of that in cold months, suggesting the two seasons introduced here capture the typical seasonal characteristics in this region reasonably well. SO₄ ~~seems to be is~~ removed less efficiently than Org and eBC during warmer months during the arrival of the airmasses to SMEAR II, as can be seen from Figure 4d. During the first 10 mm of accumulated precipitation, the normalized particle mass has decreases from 1 to 0.62 for SO₄, whereas Org and eBC have reached 0.37 and 0.32, respectively. This is surprising as sulfate is more hygroscopic than Org and eBC. There are two possible explanations for the observed differences. First, ~~t~~This could indicate that more of the SO₄, compared to Org and eBC, is distributed to smaller particles during warmer months. This~~which~~ reduces both CCN activation potential and ~~thus~~ removal of activated particles by rainfall. ~~The observed differences cannot be explained by below cloud scavenging, as the composition measurements are representative for particle sizes above 70 nm (up to 1 μm), which are not efficiently scavenged below cloud (e.g. Croft et al.,~~
410 ~~2009).~~ Second, Also, the stronger contribution of local sources of SO₄ during warm months could distort our analysis and result in lower derived removal efficiency.

Conversely, during the colder months (Figure 4e), SO₄ is removed slightly more efficiently than Org and BC (decreases from 1 to 0.39, 0.34 and 0.28 for Org, eBC and SO₄, respectively, with the first 10 mm of accumulated precipitation). The differences of the removal efficiency between the investigated components are smaller during colder months when compared
420 to warmer months, suggesting the species are internally mixed during colder months (as SO₄ and eBC, for example, have very different hygroscopicity, but still are removed almost as efficiently). The trajectories derived with the GDAS meteorology precipitate, on average, less (Figure S2149) than those derived with the ERA-Interim meteorology (Figure S1). This explains the less efficient derived removal of the standardized particle masses in Figure S242d-e. It is also possible that the seasonal differences in cloud types and cloud cover fractions within one grid box in the reanalysis dataset could have an
425 effect to the observed differences between the wet scavenging efficiencies. ~~The relative contribution of wet scavenging is 5-10 times smaller during the warmer months (Tables S4-S6), which show less defined removal by accumulated precipitation compared to warmer months. Regression coefficients indicate more efficient removal during colder months for all species.~~ Comparing Figure 4d and e, we see that the data points are much more scattered during the warmer months for all three species. This could indicate a larger contribution from local production and thus we can observe relatively large mass
430 concentrations in SMEAR II even with high accumulated precipitation values along the airmass route. Based on the mixed effects model, the relative contribution of wet scavenging is 5-10 times smaller during the warmer months (Tables S7-S9),

which show less defined removal by accumulated precipitation compared to warmer months. Regression coefficients indicate more efficient removal during colder months for all species (Tables S10-S12). Figure S98 shows the particle number size distribution for $d_p = 50\text{-}700$ nm (electrical mobility diameter), roughly representative for the sizes measured by ACSM (ca. 75-1000 nm in vacuum aerodynamic diameter) as a function of the accumulated precipitation (like Figure 3a) for the two temperature regimes. We clearly observe a relatively high number of particles, especially smaller ones, during warmer months despite the high values of accumulated precipitation along the trajectory. The decreases seen in the number size distribution for the different particle sizes during the first 10 mm of precipitation are steeper during the colder months. Similar behaviour (steeper decrease during colder months) is observed for SO_4 mass concentration in Figure 4e. Based on the statistical modelling, the contribution of local meteorology to the organic mass concentration, for example, is an order of magnitude larger during warmer months (group 3 in Table S74). For SO_4 and eBC, large difference between the seasons is seen in terms of long-range transport (group 5 in Table S85 and S96). Long-range transport has relatively small contribution (Section S3.22-3.2) in the mixed effects models during the warm months compared to colder months (i.e. the variable group is less crucial for the model with data from warmer months), and as the wet scavenging discussed here takes place along the airmass route, defined removal is not observed (as seen in Figure 4d). Conversely, during cold months the relative contribution of long-range transport (and wet scavenging, group 4a) for SO_2 is much larger, thus we see more defined removal (i.e. less scattering of the data points) during the colder months in Figure 4e for eBC and SO_4 .



450

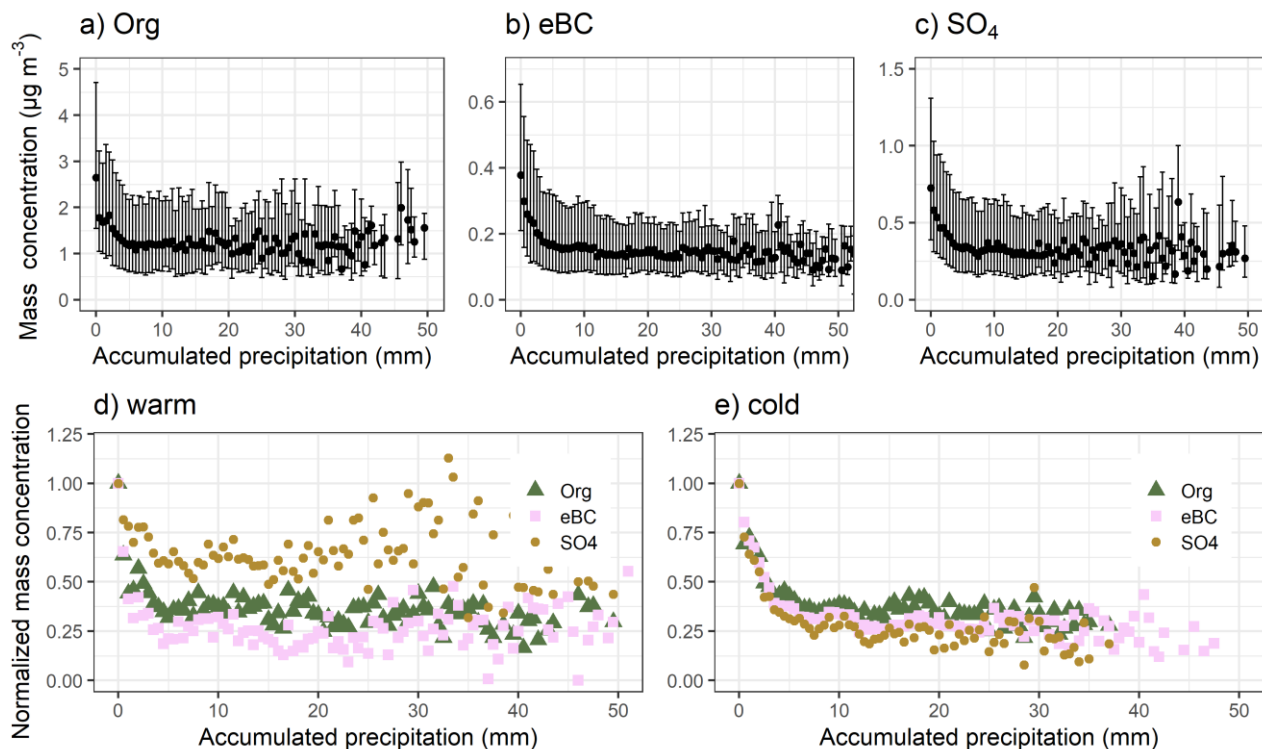


Figure 4 Particle mass concentration of a) Org, b) eBC and c) SO₄ as a function of accumulated precipitation along the 96-hour HYSPLIT airmass trajectories from all seasons. The black dots in the top row show the median values and bars highlight the 25th-75th percentiles for each 0.5 mm bin of accumulated precipitation. Bottom row shows normalized particle masses (calculated from the medians) with temperature separation. Medians and normalized medians are shown for each bin having 10 or more data points. The figure includes data between 2006-2019 for eBC and 2012-2019 for Org and SO₄.

3.3 Effect of in-cloud processing on aerosol concentrations and composition

To investigate the possible effects of in-cloud processing on aerosol composition, we took advantage of the relative humidity (RH) provided by the HYSPLIT model along the airmass trajectories as described in Section 2.2. We selected a limit of RH > 94 % (similar to Tunved et al., 2004) to identify cases that we assume the airmass is inside a cloud (or fog, as we do not separate these cases) as visualized in Figure 2. We would like to note that even if the approximation for the in-cloud cases is not very accurate based on the RH values only, the humidity in these cases is high enough for the particles to have taken up significant amounts of water. Strong hygroscopic growth can be observed before activation, and e.g. for inorganic salts the deliquescence RH is well below 94 % (e.g. Cruz and Pandis, 2000; Zieger et al., 2017; Lei et al., 2018). Thus, it is safe to assume the aqueous phase processes, whether in cloud or inside fogs, are taking place when RH of 94 % is exceeded.

The observations were divided into 3 groups based on the conditions (precipitation and clouds) the arriving airmasses have experienced during the last 24 hours to investigate if precipitation and in-cloud aqueous phase processing affect the particles

differently. Group 1 represents the cases where the arriving airmasses have not experienced precipitation or clouds (i.e. $RH < 94\%$) within the last 24 hours before arriving at SMEAR II. Group 2 represents cases where airmasses have experienced precipitation within the last 24 hours. Group 3 represents cases where the airmass has experienced $RH > 94\%$ (i.e. in-cloud conditions) but no precipitation within the last 24 hours. These definitions are summarized in [Table 1](#)[Table-2](#). We restrict trajectories to the 24 hours prior to arrival to ensure enough observations corresponding to the trajectories in each group, especially in [gGroup 3](#) which has the strictest criteria. [With longer trajectories, more of the trajectories would contain precipitating clouds, which would lead to a reduction of observations in group 3. Sensitivity analysis was conducted by limiting airmass experience to 36 and 48 hours, but same conclusions were achieved.](#) [Figure 5](#) shows the median mass (a) and number (b) concentration of the accumulation mode ($d_p = 100-1000$ nm) particles based on their experiences of precipitation and high humidity conditions ($RH > 94\%$) during the last day before arrival to SMEAR II, as described in [Table 1](#)[Table-2](#). [Mann-Whitney U test \(Mann and Whitney, 1947\) was applied to assess the statistical significance of the differences between the groups.](#) [Figure 5b](#) shows that the accumulation mode number concentration is lower if the airmass has experienced precipitation (group 2) or high humidity conditions (i.e. clouds) without precipitation (group 3), compared to the case when the airmass has not experienced precipitation or in-cloud conditions (group 1). When the mass concentration ([Figure 5a](#)) is investigated, we see higher mass concentration for group 3 compared to group 1, suggesting that in non-precipitating, high RH conditions the aerosol mass increases due to aqueous phase processes. [The observed differences between the wet processing groups for both mass and number concentration were statistically significant \(Table S4\).](#) Identical observations can be made if the GDAS reanalysis meteorology is used in the calculation of the trajectories ([Figure S253](#)).

To investigate further the observed increase in accumulation mode mass concentration ([Figure 5a](#)) when the airmass had experienced high humidity conditions, we investigated the bulk aerosol composition. We focus on group 1 (no wet processing at all) and group 3 (high humidity conditions, but no precipitation) as we are now interested in the increase in mass concentration between those groups, as shown in [Figure 5a](#). Here, we concentrate on the mass concentrations of organics (Org) and sulfate (SO_4), and black carbon (eBC) measurement data. [Figure 6](#) shows the median particle mass concentrations (see [Fig. S109](#) for mass fractions) for each of these chemical species for clean and more polluted airmasses with the temperature division for the wet processing groups 1 and 3. The division of the trajectories into “clean” and “polluted” sectors was made by assigning any trajectories that visited latitudes below 60 degrees North into polluted sector, and rest to the clean. Thus, our final subgroups are WC (warm, clean), WP (warm, polluted), CC (cold, clean) and CP (cold, polluted). This approach was applied to make sure the observed changes in the concentration of species are indeed related to the aqueous phase processing and to exclude the influence of artefacts arising from possible association of different source areas to different meteorological conditions (i.e. group 1 vs group 3). [This type of source area artefact could take place, for example, if cloud occurrence would be more frequent for airmasses arriving from certain directions, which could \(randomly\) coincide with higher \$SO_4\$ observations.](#) Further justification for our choice of these sectors can be found in the chapter below. [Statistically significant \(Table S5\) increases exceeding the error limits \(except subgroup WC, which shows a small](#)

decrease) in SO₄ concentration (Figure 6) are observed between wet processing groups 1 and 3, suggesting SO₄ formation in the aqueous phase, while no significant changes are observed for Org. Black carbon shows both increases and decreases in mass, depending on the subgroup, and eBC, except for CP subgroup (Figure 6d) where Org shows a decrease. The patterns in the mass concentrations for each species between the groups 1 and 3 showed similar behaviour when we increase the time (0-24 h into e.g. 0-36 h or 0-48 h) used to determine the classes.

Table 12 Definitions for the wet processing groups. Availability shows the percentage of trajectories relative to total number of trajectories belonging to the wet processing groups.

Group	History during the last 0-24 hours before arrival to SMEAR II	Quick summary	Availability (%)
1	Airmass has not experienced precipitation or RH > 94%	No precipitation or in-cloud processing	24.5
2	Airmass has experienced precipitation	Wet scavenging	62.2
3	Airmass has experienced RH > 94 % but not precipitation	Only non-precipitating clouds (in-cloud processing)	13.3

*Definitions are according to description of explained quantities in Sect. 2.2

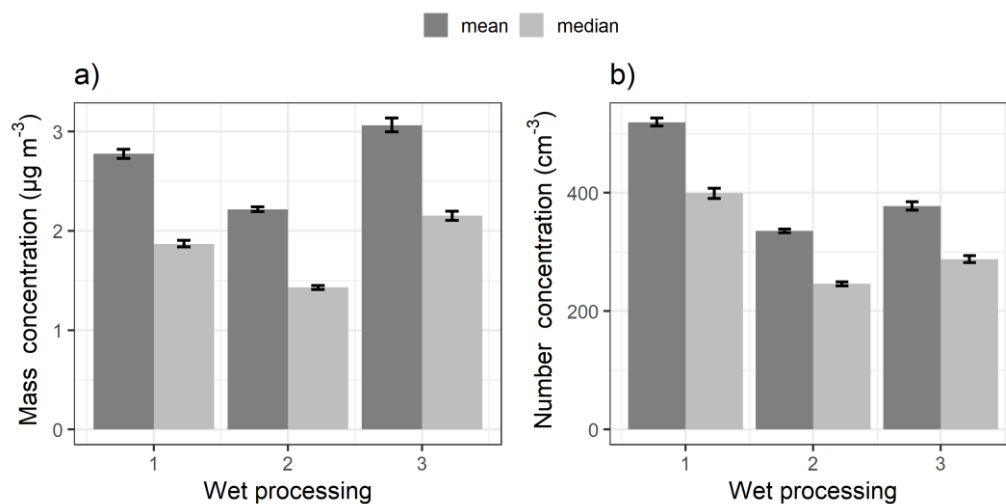
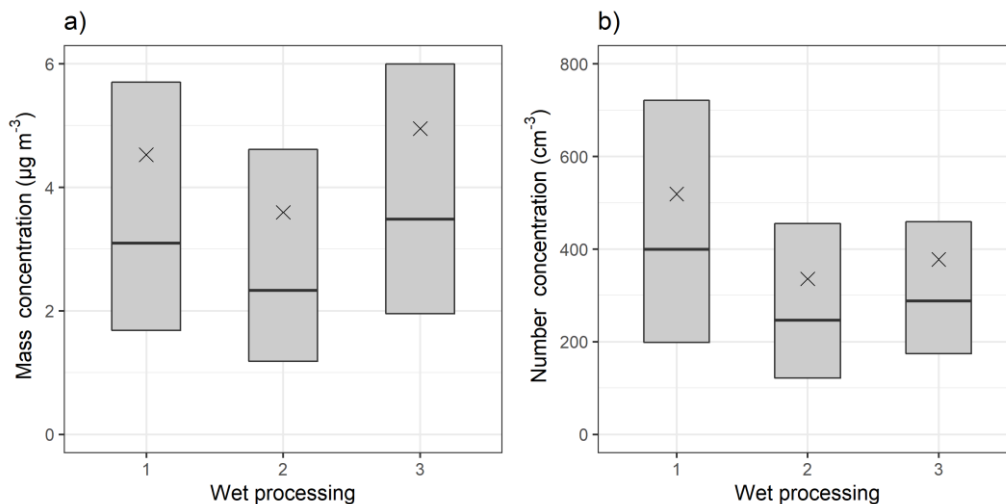


Figure 2 Median and mean accumulation mode ($d_p = 100-1000$ nm) particle mass (a) and number (b) concentration for wet processing groups described in Table 2. The figure includes DMPS data between January 2005 and August 2019. The whiskers show the 99% confidence intervals from 1000 bootstrap replicates.



515

Figure 5 Median (black horizontal lines), mean (black crosses) and 25th-75th percentiles (boxes) for accumulation mode ($d_p = 100$ -1000 nm) particle mass (a) and number (b) concentration for wet processing groups described in Table 1. The figure includes DMPS data between January 2005 and August 2019.

520 Two sectors were used to distinguish the more polluted and mostly clean airmasses, as more detailed division on air mass source areas is not possible because of the limited amount of data available especially for the group 3 cases. Even though the division is relatively rough, it does separate the airmasses quite well, especially as we have already excluded the highly polluted airmasses arriving from the Kola peninsula and emissions arriving from the nearby sawmills. For example, in a former study from Kulmala et al. (2000), trajectories arriving from the Arctic ocean coincide with a low number of accumulation mode particles and low SO_2 concentration and, therefore, airmasses arriving from that sector are classified as “clean”. Sogacheva et al. (2005) also presented similar sources for accumulation mode particles. The same classification is used in this study. Sectors from Kulmala et al. (2000) including the southeast of Russia and Central Europe showed highest accumulation mode number and SO_2 concentrations and are classified as “polluted” also in our study. We selected two sectors to maintain high enough statistics for the composition measurements to achieve reliable results. In addition, the temperature-based division, discussed in section 3.1, gives additional insight when separating the airmasses. Riuttanen et al. (2013), conducted trajectory analysis to investigate trace gases observed in SMEAR II, and our temperature-based division coincides well with the seasonality of SO_2 concentration. They concluded, for example, that combustion related SO_2 is mainly transported to SMEAR II from Eastern Europe during winter months. In addition, for high particle concentrations arriving to SMEAR II, they observed the airmass origins to be dependent on particle size.

535 To further confirm that the seasonal patterns of trace gases like SO_2 and aerosols shown in Riuttanen et al. (2013) also hold for our study period, source contribution analysis was conducted. No major changes in the source areas are observed (Figure

S175 and Figure S186 as examples for accumulation mode particle number concentration and SO₂ mixing ratio, respectively) when compared to the study from Riuttanen et al. (2013). We can observe a clear difference in the total mass concentration between clean and more polluted airmasses in Figure 6, indicating our sector division into mainly clean and more polluted is suitable. The average particle number size distribution with these sector- and temperature-based divisions is shown in Figure S110, but reader should be aware that the composition measurements do not represent particles with d_p < 70 nm. There is no clear difference in the geographical distribution of air mass trajectories between the wet processing groups 1 and 3 shown in Figure 7, thus we can conclude that the observed differences in SO₄ are not associated to different source areas of airmasses between the groups 1 and 3. Group 3 includes fewer trajectories due to our strict definitions of the airmass history groups, but the trajectories are arriving from similar areas in both group 1 and group 3. Further, to show that the increase in sulfate concentrations is driven by sulfate formed mostly in the clouds and not just directly above the sea surface derived for example, from dimethyl sulfide emissions exclude possible influence caused by transport of SO₄ from the oceans into our results (e.g. dimethyl sulfide derived sulfate aerosols, which could show up as high SO₄ concentrations coinciding with high humidity conditions if the airmass trajectory passes close to the sea surface, (e.g. Barnes et al., 2006), we investigated the vertical transport of the airmasses. This analysis showed no evidence (see Section S4) that this type of transport is significantly influencing the results presented here.

Thus, based on the airmass history analysis presented above and conclusions drawn regarding SO₄ transport from oceans, we can state that the observed increase in SO₄ is likely due to aqueous phase chemistry, where SO₂ is oxidized in the aqueous phase to form SO₄ (e.g. Barth et al., 2000; Ervens, 2015; McVay and Ervens, 2017). A relative increase of 45-63 % is observed between groups 1 and 3 in Figure 6b-d (airmass histories WP, CC, CP), and the largest increase is observed for more polluted airmasses during colder months (CP). The increase in SO₄ concentration is not seen for clean airmasses during the warmer months (Figure 6a, WP) as e.g. SO₂ concentration, an important precursor for SO₄ formation in-cloud, are lower in cases for airmasses coming from northern areas and for the warm season (Kulmala et al., 2000; Riuttanen et al., 2013). For the colder months and more polluted airmasses (Figure 6b-d), the increase in SO₄ is more pronounced due to more precursor SO₂ available for SO₄ production in-cloud (e.g. Paulot et al., 2017). The increasing trends in SO₄ mass concentration and mass fraction are similar to what is shown in Figure 6, when all chemical species measured by the ACSM are considered (mass concentrations in Figure S121, mass fractions in Figure S132). In addition, small increases in the mass concentration of -NH₄ can be observed for group 3. This is likely because of the enhanced uptake of ammonia from the gas phase with increasing sulfate fraction (Harris et al., 2014). Changes in the SO₄ concentration due to aqueous phase processing are similar also when the GDAS reanalysis meteorology is used. In-cloud formation of SO₄ is also supported by the statistical model in which we consider the other factors also affecting the local particle concentrations (Table S118).

The median mass concentration of Org shows no difference or decrease when comparing case 1 to case 3 in Figure 6a, b and d, but no change - e but shows a decrease in the cold and clean/polluted subgroup (Figure 6cd, CCP, relative decrease 32%). However, the observed decreases were not statistically significant (Table S5) at the $\alpha = 0.01$ limit. With trajectories using GDAS reanalysis meteorology, decreases in the median mass are also observed for the same subgroups decrease in Org

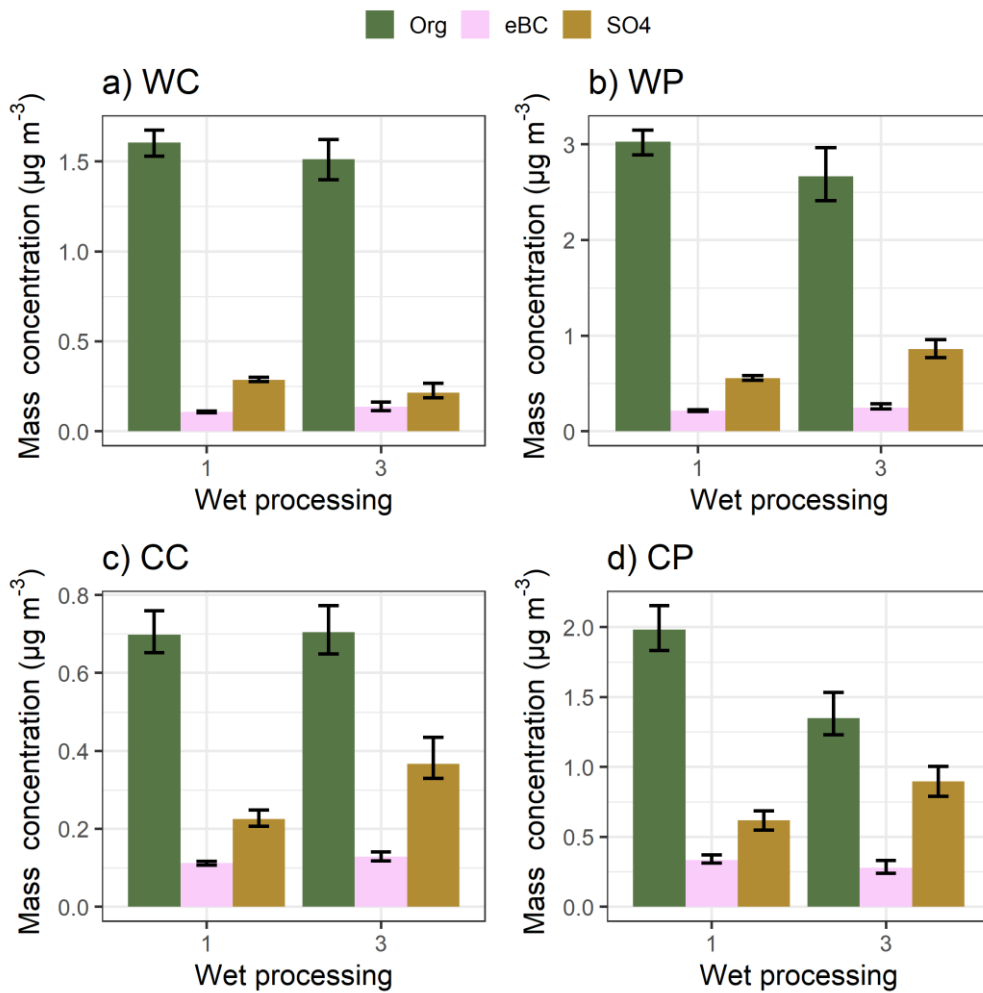
exceeding the error limits is also seen, but for the warm and clean airmasses (Figure S24a, WC). Previous studies have shown an increase of organic mass through aqueous phase production of SOA (Blando and Turpin, 2000; Ervens and Volkamer, 2010; Ervens et al., 2018). For example, Ervens et al. (2018) investigated the formation of aqSOA with parcel models from gas-phase precursors of toluene, xylene, and ethylene. In SMEAR II, the gas phase precursors from biogenic sources are dominated by monoterpenes specially during warm months (e.g. Hakola et al., 2012; Patokoski et al., 2015; Barreira et al., 2017; Heikkinen et al., 2021).

During the colder months (Figure 6c-d), the airmasses are likely to have more anthropogenic influences and thus a different VOC profile (e.g. Patokoski et al., 2015), but the formation of aqSOA is still negligible when the total Org mass is investigated in this area of northern Europe. It has also been suggested that water soluble SOA (originating from other sources than aqueous phase processing) in the cloud droplets can become oxidized ~~and become more to form more~~ volatile compounds leading to evaporation. This could lead to a decrease in total SOA mass, even though additional the aqueous phase SOA mass is formed (Ervens et al., 2018). In addition, the increase in SO₄ can increase the acidity of the droplets which might increase the evaporation of organic acids leading to a decrease in the organic mass (Ervens et al., 2018). Our data suggests that the local photochemically driven SOA production at SMEAR II (and surrounding areas) dominates over the aqueous phase SOA formation especially during the warm months. This is supported by the solar radiation values measured at SMEAR II (not shown), as they are much lower for group 3 than for group 1 for all cases. Hence, decreased SOA formation due to the decreased photochemical activity could compensate for the in-cloud aqueous phase SOA formation resulting in comparable total organic mass when groups 1 and 3 are compared. Our results indicate, that in the boreal forest dominated Northern Europe the photochemical SOA formation in the gas phase dominates over SOA formation in the aqueous phase. in-cloud aqueous phase SOA production has negligible impact on total observed when the total organic mass is considered. This applies for both during warmer and colder seasons, and in the case of clean and polluted airmasses. The Org mass concentration also shows no increase due to clouds when the other factors affecting the local concentrations are considered with the mixed effects model (Table S107).

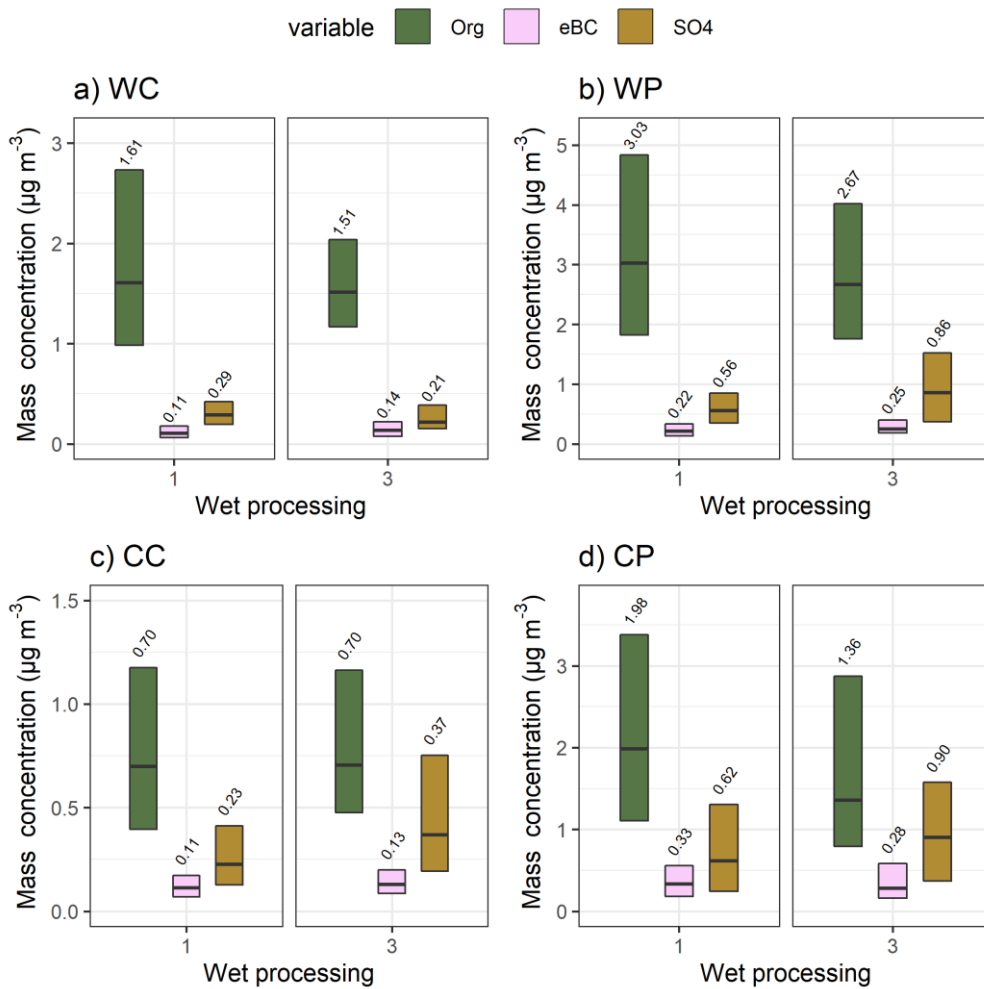
When investigating the composition of the particles as a function of time in RH > 94 % (Figure 8) when no distinction relative to precipitation is applied (i.e. time in cloud can also include precipitating clouds), we observe an increase in sulfate mass fraction with time spent under the high humidity conditions. This is most clear, especially for the more polluted airmasses which also have more SO₂ available for the in-cloud production of SO₄ (Figure 8a). This trend is not seen when looking at the time the air mass was influenced by precipitation (Figure 8b) indicating precipitation acts mainly as a sink for the particles, whereas high humidity conditions, i.e. in-cloud aqueous phase processing, also alters the particle chemical composition. Inspection of the absolute mass of the species (Figure S14) also shows an increase in SO₄ mass with longer exposure times in RH > 94 %, whereas decreases in mass of all species is seen with increasing time of experienced precipitation. Again, the increasing trend in SO₄ fraction when the airmasses arrive from cleaner areas is more subtle (Figure 8c). Same trends are observed when all species from the composition measurements are investigated (Figure S153). These results suggest that not only the experience of in-cloud aqueous phase processing (Figure 6) affects the particle

605 composition, but also the time spent in cloud has an effect. Unfortunately, with this type of analysis of the time dimension, we were not able to apply the temperature-based division in addition to the sector division as it would limit the number of observations for the long exposure times too much to obtain statistically reliable results. Results obtained with the GDAS reanalysis meteorology (Figure S286) agree well with those from Figure 8. The very long exposure times (> 60 hours) of precipitation are missing from the GDAS derived trajectories due to lower occurrence of precipitation events compared to
610 the ERA-Interim derived trajectories (see Figures S1 and S2149).

To investigate which particle sizes are most affected by the increasing mass of SO₄, the DMPS size distribution was divided into 7 classes with particle dry diameter ranges (in nm) of [3, 30], (30, 50], (50, 100], (100, 200], (200,350], (350, 600] and (600, 1000]. Using the air mass history groups presented in [Table 1](#)[Table 2](#), the mass concentrations for these size classes are shown in [Figure 9](#) corresponding to the sector and temperature divisions first shown in [Figure 6](#). The mass concentration is
615 larger if the air mass has experienced high humidity conditions (group 3) for particle with diameters between 200-1000 nm, when compared to group 1 where there have not been any wet processes in the last 24 hours. Same observation can be made with the trajectories using GDAS meteorology (Figure S297). The increase is clearest in size ranges (200, 350] and (350, 600] and the size range (600, 1000] shows a very minor increase in mass for some subgroups. The changes in mass are also statistically significant except for sector CP for size range (200, 350] and (600, 1000] (Table S6). The same changes are also
620 seen when the particle mass data is strictly limited to simultaneous observations with the composition (Org, SO₄, BC) measurements (Figure S164). These results suggest that the SO₄ formed via in-cloud aqueous phase processes is mainly distributed to particles having a dry diameter between 200 - 1000 nm.



625 **Figure** Median particle mass concentration for Org, eBC and SO₄ for wet processing groups 1 and 3 as described in Table 2. Subplots show the air mass sectors (clean and polluted) with the seasonal (warm and cold) division following: a) warm and clean, b) warm and polluted, c) cold and clean and b) cold and polluted. The figure is based on simultaneous observations of these three species between March 2012 and August 2019. The whiskers show the 99 % confidence intervals from 1000 bootstrap replicates. Note the different y-axis limits in each subplot.



630

Figure 6 Median (black horizontal lines and numerical values) particle mass concentration with 25th-75th percentiles (boxes) for Org, eBC and SO₄ for wet processing groups 1 and 3 as described in Table 1. Subplots show the air mass sectors (clean and polluted) with the seasonal (warm and cold) division: a) warm and clean, b) warm and polluted, c) cold and clean and b) cold and polluted. The figure is based on simultaneous observations of these three species between March 2012 and August 2019. Note the different v-axis limits in each subplot.

635

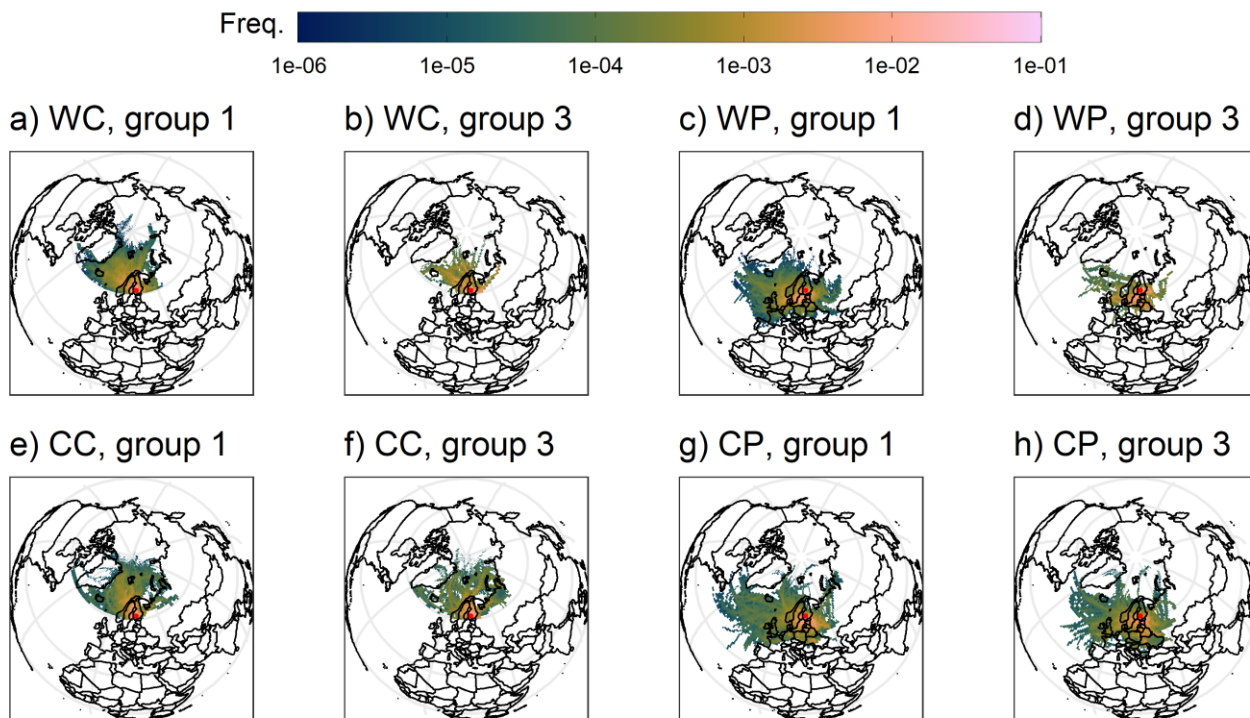


Figure 96-hour air mass history for the wet processing groups (1 and 3) with the sector (clean and polluted) and temperature (warm and cold) division. Subplots show a) b) warm and clean, c) d) warm and polluted, e) f) cold and clean and g) h) cold and polluted. Colour scale shows the frequency (crossings in each 1° x 1° grid point divided by total number of crossings in each group) of trajectories crossing a grid point. The groups 1 and 3 correspond to the air mass history groups presented in Table 2. The red dot shows the location for SMEAR II.

640

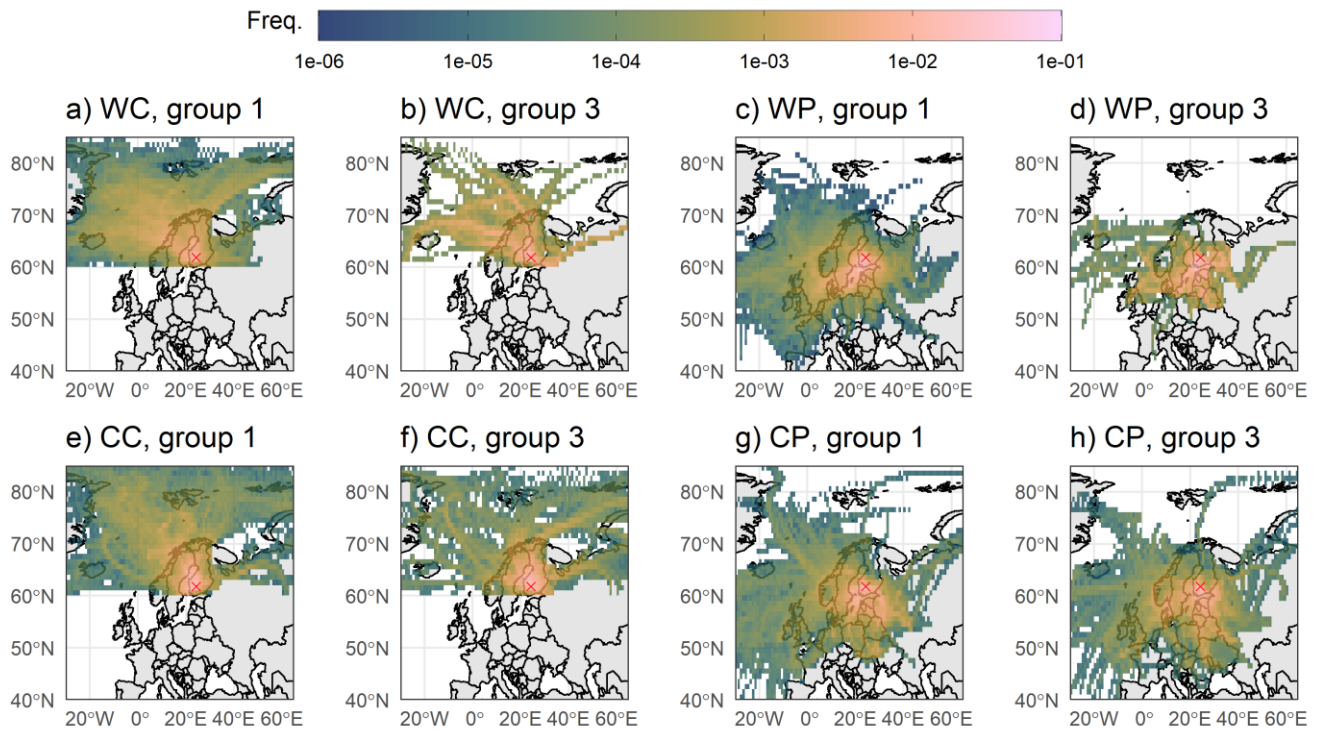
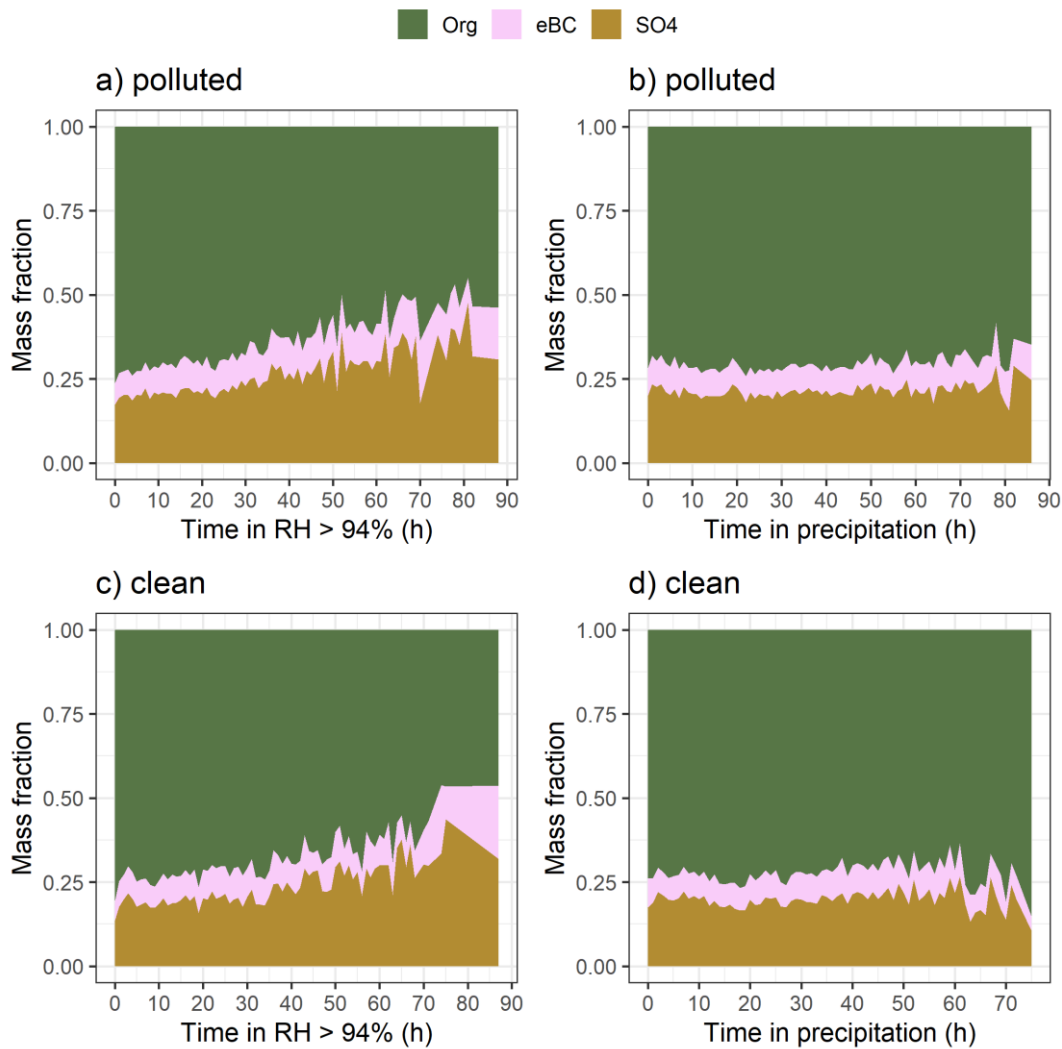


Figure 7 96-hour airmass history for the wet processing groups (1 and 3) with the sector (clean and polluted) and temperature (warm and cold) division. Subplots show a)-b) warm and clean, c)-d) warm and polluted, e)-f) cold and clean and g)-h) cold and polluted. Colour scale shows the frequency (crossings in each 1° x 1° grid point divided by total number of crossings in each group) of trajectories crossing a grid point. The groups 1 and 3 correspond to the airmass history groups presented in Table 1. The red cross shows the location for SMEAR II.

645



650

Figure 8 The mass fractions of Org, SO₄ and eBC for clean and more polluted airmasses as a function of time spent in RH > 94 % (a and c) and in precipitation (b and d): Figure shows median values for each 1-hour bin, if 10 or more data points were available in the bin. The figure is based on observations between March 2012 and August 2019.

655

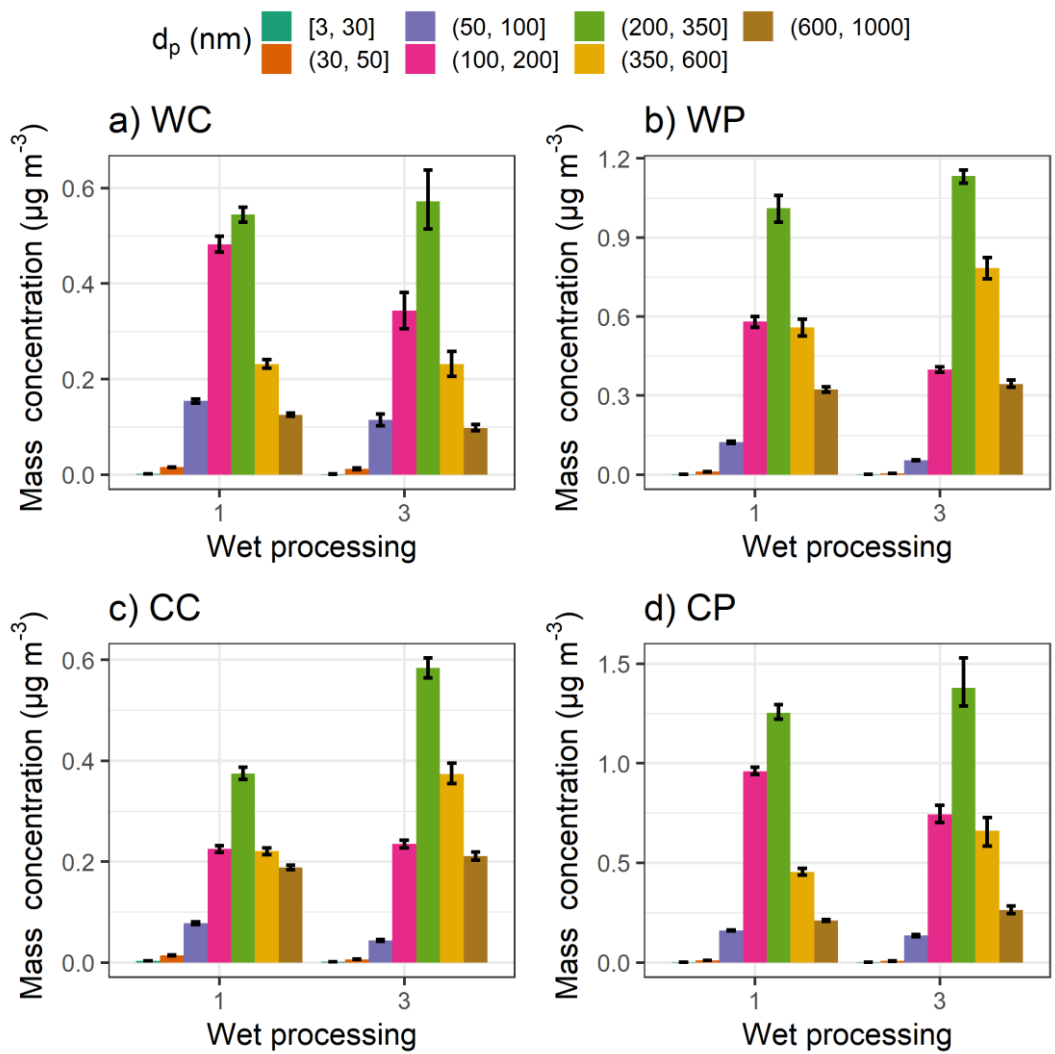


Figure Median particle mass concentration for size bins derived from the DMPS measurements for wet processing groups 1 and 3 as described in Table 2. Subplots show the air mass sectors (clean and polluted) with the seasonal (warm and cold) division followingly: a) warm and clean, b) warm and polluted, c) cold and clean and b) cold and polluted. The figure includes all available data between January 2005 and August 2019. The whiskers show the 99 % confidence intervals from 1000 bootstrap replicates. Note the different y-axis scale in each subplot.

660

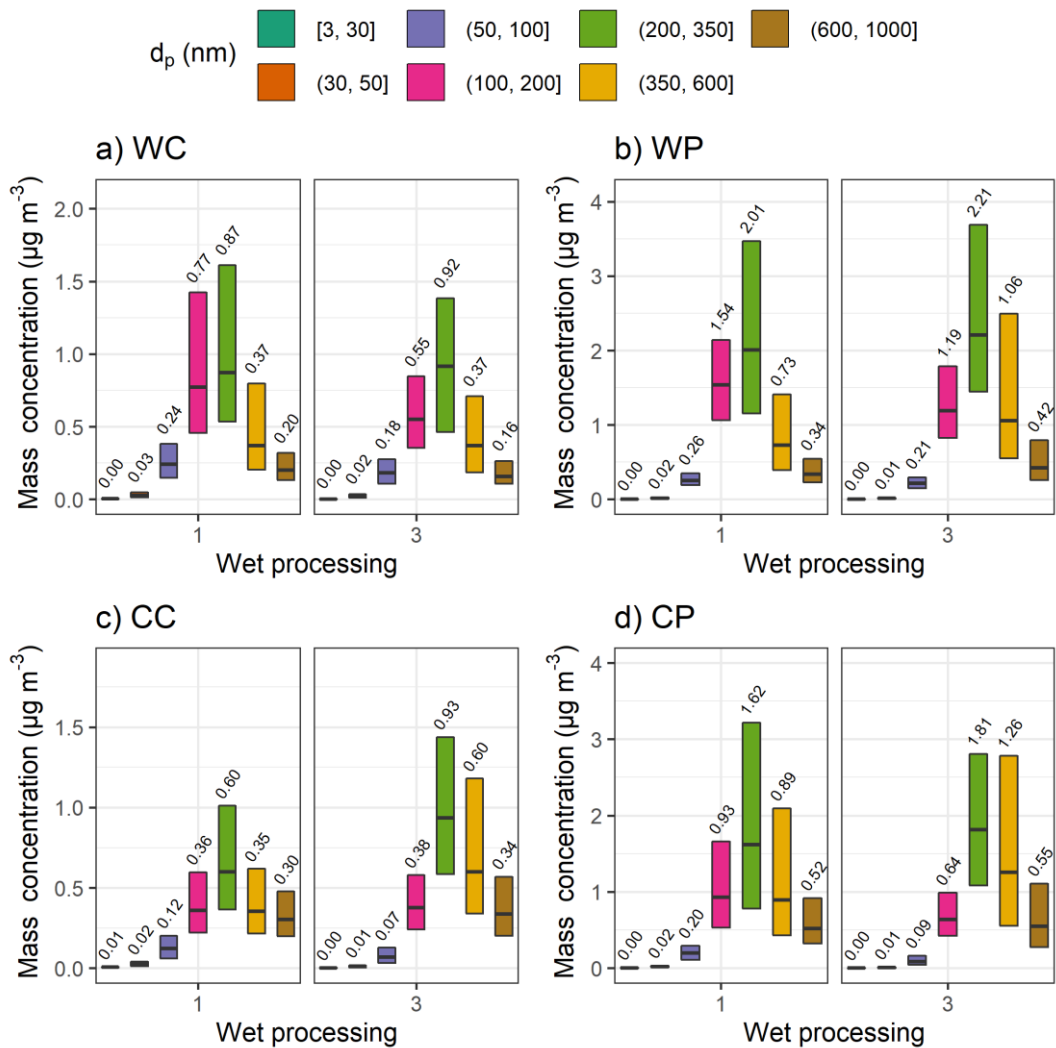


Figure 9 Median (black horizontal lines and numerical values) particle mass concentration with 25th-75th percentiles (boxes) for size bins derived from the DMPS measurements for wet processing groups 1 and 3 as described in Table 1. Subplots show the air mass sectors (clean and polluted) with the seasonal (warm and cold) division: a) warm and clean, b) warm and polluted, c) cold and clean and b) cold and polluted. The figure includes all available data between January 2005 and August 2019. Note the different y-axis scale in each subplot.

665

4 Conclusions

670 In this study, we investigated ~~how~~ wet processes ~~taking place~~ in clouds including aerosol wet scavenging and aqueous phase oxidation along air mass trajectories. We examined how they affect ~~to~~ the observed sub-micron aerosol population in SMEAR II station, ~~Hyytiälä, Finland~~ which represents the boreal environment.

Our first objective was to investigate ~~how~~ efficiently different chemical species are removed from the atmosphere by precipitation. We observed, ~~Based on a timeseries~~ over a decade long ~~timeseries,~~ ~~we observed~~ an exponential decrease in

675 particle mass as a function of accumulated precipitation along the trajectory, similar to ~~what has been that~~ reported in earlier studies. We concluded ~~d~~ that ~~the~~ in-cloud wet scavenging dominated ~~ds~~ over below-cloud precipitation scavenging, especially for ~~particles of the~~ accumulation ~~-mode~~ size ($100 \text{ nm} < d_p < 1 \text{ }\mu\text{m}$) ~~-sized particles.~~ Scavenging of particle mass Particle mass scavenging was more effective during colder months especially for sulfate aerosol, whereas the behaviour of other

680 ~~investigated~~ aerosol chemical species ~~investigated~~ behaviour was more alike. Statistical mixed effects models also ~~showed~~ exhibited removal by accumulated precipitation for all species, suggesting more efficient removal in colder months. In addition, ~~the~~ scavenging efficiencies were relatively similar between ~~the~~ species in colder months, suggesting that the particles were internally mixed and ~~the~~ different species were distributed to similar ~~ly~~ sized particles. During warmer months, ~~it is likely that~~ strong local particle production at SMEAR II likely effectively masks ~~the~~ wet scavenging along the trajectory. Thus, despite high values of accumulated precipitation, relatively high particle mass concentrations are

685 ~~observed exist,~~ despite high values of accumulated precipitation. This finding was supported by ~~the~~ statistical modelling, wherein, for example, in which e.g. the relative contribution of local meteorology on organic aerosol production was much larger during ~~the~~ warmer months. Seasonal differences in cloud types and cloud cover fractions within one grid box in the reanalysis dataset may also have an effect influence to the ~~observed~~ differences observed between seasons in wet scavenging efficiencies between the seasons.

690 Our second objective was to investigate how aqueous phase processing occurring taking place in clouds alters ~~the~~ particle mass concentration and composition. Our study revealed eds a significant in-cloud formation of sulfate mass, but aqueous phase SOA formation could not be identified by the analysis. In-cloud processing was separated by using relative humidity as a proxy for ~~the~~ air mass with cloud experience ~~to have experienced clouds,~~ and T the precipitation data along the air masses was used to separate non-precipitating clouds. An increase in accumulation mode particle mass was observed for air masses that

695 had recently been in-cloud when compared to clear sky air masses which had ~~(air masses with~~ no experience of clouds or rain during the last 24 hours). In ~~(The~~ chemical composition of accumulation mode particles was studied and the increase observed increase in particle mass can be mostly attributed to in-cloud SO₄ production ~~of SO₄.~~ Our analysis showed eds that, due to in-cloud sulfate formation, sulfate mass concentrations increased 45 % - 63 %, depending on season and air mass origin, due to in-cloud sulfate formation. Furthermore, the increase in sulfate mass fraction was higher when the air mass had spent

700 more time in high humidity conditions. We considered, in the s Statistical mixed effects model, in which additional factors

affecting local SO₄ concentrations. ~~are considered~~; This model also supported in-cloud SO₄ formation whereas no formation of Org or eBC mass was observed.

Airmass history analysis was applied to separate airmasses originating from different sources (more polluted and mostly clean) in addition to ~~the~~ temperature-based seasonal division. Thus, we ~~to~~ investigated how different conditions along the airmass trajectories affected ~~the observed~~ increase observed in SO₄ mass concentration due to in-cloud processes. When airmasses originated from areas with more pollution sources producing gaseous SO₂, we observed a greater increase in SO₄ mass. This increase was ~~observed~~ due to more SO₂ being available in the gas phase to be oxidized in-cloud to form SO₄. ~~Increases in the total organic mass due to aqueous phase processing was not observed. Aqueous phase production of organic mass was not observed during the warm months since monoterpenes dominate both the biogenic VOCs and total VOCs in this region. In wintertime anthropogenic emissions dominate over biogenic emissions, thus aqueous phase production of organic mass was not observed during the cold months either.~~ We were also interested whether ~~if~~ the effects of aqueous phase processes were ~~are~~ different for particles of different size. Therefore, we investigated changes in ~~the~~ particle number size distribution, were investigated to determine into which particle sizes the ~~observed~~ mass increase observed in SO₄ was ~~is~~ mostly distributed. Increases in particle mass occurred ~~were observed~~ for sizes larger than 200 nm, whereas smaller sizes displayed ~~showed~~ a decrease in some cases.

Finally, as an additional robustness test for our results, we also compared the trajectories based on different reanalysis meteorologies, ~~(ERA-Interim and GDAS) as an additional robustness test for our results~~. Both approaches yielded ~~gave~~ nearly identical results, supporting and thus the same conclusions ~~could be drawn~~. Trajectories obtained with ~~the~~ GDAS reanalysis meteorology had, in general, fewer ~~less~~ precipitation events; Thus and thus, compared to that in ERA-Interim- based trajectory results, the scavenging efficiency of the investigated ~~species investigated~~ was lower, ~~compared to the results obtained with ERA-Interim based trajectories.~~ With both approaches, aqueous-phase SO₄ formation in the aqueous phase was observed to significantly contribute d to the total SO₄ mass ~~with both approaches~~ whereas aqSOA ~~formation of aqSOA~~ was un ~~not~~ detected. Precipitation values derived from the trajectory model at SMEAR II agreed ~~also~~ well with ~~the~~ locally measured precipitation. The results from this study offer ~~an~~ interesting insights into using air mass history analysis to study aerosol-cloud interactions. These findings ~~and~~ facilitates the comparison of observed aerosol wet scavenging and in-cloud processing with outcomes of larger scale models. ~~This study highlights that the ability of G~~ global models can ~~to~~ simulate aerosol composition and size distribution, especially away from source regions; This study highlights that this ability can be improved ~~enhanced~~ by improving the description of size-dependent wet removal of different aerosol compounds. Our analysis also provides a good platform for evaluating the ability of models to simulate in-cloud chemical formation of aerosol. Regarding ~~Further analysis is needed to investigate in more detailed~~ the effect of clouds and precipitation on aerosol dynamics and detailed changes in size distributions, further, in-depth investigations are imperative.

Appendix A

The formulation of the final fitted equation can be expressed as

735 $[\text{VAR}_i] = \beta_0 + \{\mathbf{b}_h + \mathbf{b}_m + \mathbf{b}_y\} + \{\beta_1[\text{NOx}_i] + \beta_2[\text{SO}_{2,i}] + \beta_3[\text{O}_{3,i}] + \beta_4[\text{CO}_i]\} + \{\beta_5 T_i + \beta_6[\text{MLH}_i]\} +$
 $\{\exp(\beta_7 \text{accum. precip}_i) + \beta_8 \text{time. in. cloud}_i\} + \{\beta_9 \text{emission. col. time}_i + \beta_{10} \text{time. in. land}_i + \mathbf{b}_a\}, \text{--- (A1)}$
 740 where [VAR] is now the mass concentration of either Org, SO₃ or eBC. β_0 is a model intercept, \mathbf{b}_h , \mathbf{b}_m , \mathbf{b}_y and \mathbf{b}_a are the
vectors of random intercepts for hour of the day, month, year and air mass source area, respectively, and β_1 - β_{10} are the fixed
regression coefficients. Subscript i denotes the time point i.e. one observation. Thus the predictor variables (see Section 2.1
 745 for the abbreviations) include concentrations of SO₂, CO, NO_x and O₃ (trace gases); air T and MLH (at SMEAR II derived
from the back-trajectory data) describing the local meteorology and following trajectory-derived variables: accumulated
precipitation along the trajectory (mm), time spent in high humidity conditions without simultaneous rain (“in non-
precipitating cloud”, h), emission collection time (time in mixed layer until rain event, h) and total time the air mass has spent
over land (h). In addition, the air mass source areas (obtained by clustering as explained in Section 2.2, visualised in Figure
 750 S3 and Figure S4) and observation year, month and hour of the day were included, as shown in Eq. (A1). Summary of the
used predictor variables in the regression is shown in Table A1 and each predictor variable group is separated with curly
brackets in Eq. (A1). The process leading to the selection of the response variables is explained in detail the Section S3.1.

Table A1 Predictor variables used in regression.

<u>Group</u>	<u>Name</u>	<u>Variables included</u>
<u>1</u>	<u>Base variability (diurnal, seasonal, random)</u>	<u>Observation year and month, hour of the day</u>
<u>2</u>	<u>Trace gases</u>	<u>NO_x, SO₂, O₃, CO</u>
<u>3</u>	<u>Local meteorology</u>	<u>T, MLH</u>
<u>4</u>	<u>Wet processing along the trajectory</u>	<u>Accumulated precipitation, time spent in non-precipitating cloud</u>
<u>4a</u>	<u>Wet scavenging</u>	<u>Accumulated precipitation</u>
<u>4b</u>	<u>In-cloud aqueous phase processing</u>	<u>Time spent in non-precipitating cloud</u>
<u>5</u>	<u>Long-range transport</u>	<u>Air mass source area, emission collection time, time spent above land</u>

750

755 **Data availability**

Raw data were collected by INAR, University of Helsinki. Field data (particle [number](#) size distributions, meteorological variables, black carbon, and trace gases) are available from <https://smear.avaa.csc.fi/download>. The ACSM data on aerosol composition is available at EBAS data base at <http://ebas.nilu.no/>. The pre-processed HYSPLIT trajectory data can be obtained from the corresponding author and the trajectories can be freely calculated at the webpage

760 https://www.ready.noaa.gov/HYSPLIT_traj.php.

Author contribution

A.V proposed the study and designed the research questions. S.I had the lead role in data analysis with supporting contribution from P.K and D.P. Results were interpreted by S.I, A.V, P.K, D.P, S.M, T.Y and L.H. The manuscript was
765 written by S.I. with supporting contributions from P.K, S.M, D.P and A.V. All co-authors commented and edited the manuscript. L.H. performed the ACSM measurements and data processing. K.L. performed the aethalometer measurements and data processing.

Competing interests

770 The authors declare no competing interest.

Acknowledgements

We thank technical and scientific staff in SMEAR II station. Tuomo Nieminen is gratefully acknowledged from his contribution during initial trajectory analysis.

775

Funding information

Financial support from the European Union's Horizon 2020 research and innovation programme (project FORCeS grant No. 821205, project COALA grant No. 638703), European Research Council (Consolidator grant INTERGRATE No. 865799) and Knut and Alice Wallenberg foundation (Wallenberg Academy Fellowship project AtmoRemove No 2015.0162) is
780 gratefully acknowledged. This research has also been supported by the Academy of Finland (grant No. 317373 and 317390), Academy of Finland Flagship funding (grant No. 337550) and the Academy of Finland competitive funding to strengthen university research profiles (PROFI) for the University of Eastern Finland (grant No. 325022). The work of S.I was financially supported by the University of Eastern Finland Doctoral Program in Environmental Physics, Health and Biology.

References

- 785 Aalto, P., Hameri, K., Becker, E., Weber, R., Salm, J., Makela, J. M., Hoell, C., O'Dowd, C. D., Karlsson, H., Hansson, H. C., Vakeva, M., Koponen, I. K., Buzorius, G., and Kulmala, M.: Physical characterization of aerosol particles during nucleation events, *Tellus B*, 53, 344-358, DOI 10.1034/j.1600-0889.2001.530403.x, 2001.
- Abdul-Razzak, H., and Ghan, S. J.: A parameterization of aerosol activation: 2. Multiple aerosol types, *Journal of Geophysical Research: Atmospheres*, 105, 6837-6844, <https://doi.org/10.1029/1999JD901161>, 2000.
- 790 Andronache, C.: Estimated variability of below-cloud aerosol removal by rainfall for observed aerosol size distributions, *Atmos. Chem. Phys.*, 3, 131-143, 10.5194/acp-3-131-2003, 2003.
- Andronache, C., Grönholm, T., Laakso, L., Phillips, V., and Venäläinen, A.: Scavenging of ultrafine particles by rainfall at a boreal site: observations and model estimations, *Atmos. Chem. Phys.*, 6, 4739-4754, 10.5194/acp-6-4739-2006, 2006.
- 795 Bae, S. Y., Park, R. J., Kim, Y. P., and Woo, J.-H.: Effects of below-cloud scavenging on the regional aerosol budget in East Asia, *Atmospheric Environment*, 58, 14-22, <https://doi.org/10.1016/j.atmosenv.2011.08.065>, 2012.
- Barnes, I., Hjorth, J., and Mihalopoulos, N.: Dimethyl Sulfide and Dimethyl Sulfoxide and Their Oxidation in the Atmosphere, *Chem Rev*, 106, 940-975, 10.1021/cr020529+, 2006.
- Barreira, L. M. F., Duporte, G., Parshintsev, J., Hartonen, K., Jussila, M., Aalto, J., Back, J., Kulmala, M., and Riekkola, M.
- 800 L.: Emissions of biogenic volatile organic compounds from the boreal forest floor and understory: a study by solid-phase microextraction and portable gas chromatography-mass spectrometry, *Boreal Environ Res*, 22, 393-413, 2017.
- Barth, M. C., Rasch, P. J., Kiehl, J. T., Benkovitz, C. M., and Schwartz, S. E.: Sulfur chemistry in the National Center for Atmospheric Research Community Climate Model: Description, evaluation, features, and sensitivity to aqueous chemistry, *Journal of Geophysical Research: Atmospheres*, 105, 1387-1415, <https://doi.org/10.1029/1999JD900773>, 2000.
- 805 Bates, D., Mächler, M., Bolker, B., and Walker, S.: Fitting Linear Mixed-Effects Models Using lme4, *Journal of Statistical Software; Vol 1, Issue 1 (2015)*, 10.18637/jss.v067.i01, 2015.
- Blanco-Alegre, C., Castro, A., Calvo, A. I., Oduber, F., Alonso-Blanco, E., Fernández-González, D., Valencia-Barrera, R. M., Vega-Maray, A. M., and Fraile, R.: Below-cloud scavenging of fine and coarse aerosol particles by rain: The role of raindrop size, *Quarterly Journal of the Royal Meteorological Society*, 144, 2715-2726, 10.1002/qj.3399, 2018.
- 810 Blando, J. D., and Turpin, B. J.: Secondary organic aerosol formation in cloud and fog droplets: a literature evaluation of plausibility, *Atmospheric Environment*, 34, 1623-1632, [https://doi.org/10.1016/S1352-2310\(99\)00392-1](https://doi.org/10.1016/S1352-2310(99)00392-1), 2000.
- 815 Chate, D. M., Rao, P. S. P., Naik, M. S., Momin, G. A., Safai, P. D., and Ali, K.: Scavenging of aerosols and their chemical species by rain, *Atmospheric Environment*, 37, 2477-2484, 10.1016/S1352-2310(03)00162-6, 2003.
- Chate, D. M., and Devara, P. C. S.: Parametric study of scavenging of atmospheric aerosols of various chemical species during thunderstorm and nonthunderstorm rain events, *Journal of Geophysical Research: Atmospheres*, 110, 10.1029/2005jd006406, 2005.
- 820 Chen, Y., Wild, O., Wang, Y., Ran, L., Teich, M., Größ, J., Wang, L., Spindler, G., Herrmann, H., van Pinxteren, D., McFiggans, G., and Wiedensohler, A.: The influence of impactor size cut-off shift caused by hygroscopic growth on particulate matter loading and composition measurements, *Atmospheric Environment*, 195, 141-148, <https://doi.org/10.1016/j.atmosenv.2018.09.049>, 2018.
- Cramer, F., Shephard, G. E., and Heron, P. J.: The misuse of colour in science communication, *Nature Communications*, 11, 5444, 10.1038/s41467-020-19160-7, 2020.
- 825 Croft, B., Lohmann, U., Martin, R. V., Stier, P., Wurzler, S., Feichter, J., Posselt, R., and Ferrachat, S.: Aerosol size-dependent below-cloud scavenging by rain and snow in the ECHAM5-HAM, *Atmos. Chem. Phys.*, 9, 4653-4675, 10.5194/acp-9-4653-2009, 2009.
- Croft, B., Lohmann, U., Martin, R. V., Stier, P., Wurzler, S., Feichter, J., Hoose, C., Heikkilä, U., van Donkelaar, A., and
- 830 Ferrachat, S.: Influences of in-cloud aerosol scavenging parameterizations on aerosol concentrations and wet deposition in ECHAM5-HAM, *Atmos. Chem. Phys.*, 10, 1511-1543, 10.5194/acp-10-1511-2010, 2010.

- Cruz, C. N., and Pandis, S. N.: Deliquescence and Hygroscopic Growth of Mixed Inorganic–Organic Atmospheric Aerosol, *Environ Sci Technol*, 34, 4313-4319, 10.1021/es9907109, 2000.
- 835 Dadashazar, H., Alipanah, M., Hilario, M. R. A., Crosbie, E., Kirschler, S., Liu, H., Moore, R. H., Peters, A. J., Scarino, A. J., Shook, M., Thornhill, K. L., Voigt, C., Wang, H., Winstead, E., Zhang, B., Ziemba, L., and Sorooshian, A.: Aerosol responses to precipitation along North American air trajectories arriving at Bermuda, *Atmos. Chem. Phys.*, 21, 16121-16141, 10.5194/acp-21-16121-2021, 2021.
- 840 Dee, D. P., Uppala, S. M., Simmons, A. J., Berrisford, P., Poli, P., Kobayashi, S., Andrae, U., Balmaseda, M. A., Balsamo, G., Bauer, P., Bechtold, P., Beljaars, A. C. M., van de Berg, L., Bidlot, J., Bormann, N., Delsol, C., Dragani, R., Fuentes, M., Geer, A. J., Haimberger, L., Healy, S. B., Hersbach, H., Hólm, E. V., Isaksen, I., Kållberg, P., Köhler, M., Matricardi, M., McNally, A. P., Monge-Sanz, B. M., Morcrette, J.-J., Park, B.-K., Peubey, C., de Rosnay, P., Tavolato, C., Thépaut, J.-N., and Vitart, F.: The ERA-Interim reanalysis: configuration and performance of the data assimilation system, *Quarterly Journal of the Royal Meteorological Society*, 137, 553-597, <https://doi.org/10.1002/qj.828>, 2011.
- 845 Drinovec, L., Močnik, G., Zotter, P., Prévôt, A. S. H., Ruckstuhl, C., Coz, E., Rupakheti, M., Sciare, J., Müller, T., Wiedensohler, A., and Hansen, A. D. A.: The "dual-spot" Aethalometer: an improved measurement of aerosol black carbon with real-time loading compensation, *Atmos. Meas. Tech.*, 8, 1965-1979, 10.5194/amt-8-1965-2015, 2015.
- 850 Duplissy, J., DeCarlo, P. F., Dommen, J., Alfarra, M. R., Metzger, A., Barmapadimos, I., Prevot, A. S. H., Weingartner, E., Tritscher, T., Gysel, M., Aiken, A. C., Jimenez, J. L., Canagaratna, M. R., Worsnop, D. R., Collins, D. R., Tomlinson, J., and Baltensperger, U.: Relating hygroscopicity and composition of organic aerosol particulate matter, *Atmos. Chem. Phys.*, 11, 1155-1165, 10.5194/acp-11-1155-2011, 2011.
- Dusek, U., Frank, G. P., Hildebrandt, L., Curtius, J., Schneider, J., Walter, S., Chand, D., Drewnick, F., Hings, S., Jung, D., Borrmann, S., and Andreae, M. O.: Size Matters More Than Chemistry for Cloud-Nucleating Ability of Aerosol Particles, *Science*, 312, 1375-1378, doi:10.1126/science.1125261, 2006.
- 855 El-Sayed, M. M. H., Wang, Y., and Hennigan, C. J.: Direct atmospheric evidence for the irreversible formation of aqueous secondary organic aerosol, *Geophysical Research Letters*, 42, 5577-5586, <https://doi.org/10.1002/2015GL064556>, 2015.
- Ervens, B., and Volkamer, R.: Glyoxal processing by aerosol multiphase chemistry: towards a kinetic modeling framework of secondary organic aerosol formation in aqueous particles, *Atmos. Chem. Phys.*, 10, 8219-8244, 10.5194/acp-10-8219-2010, 2010.
- 860 Ervens, B., Turpin, B. J., and Weber, R. J.: Secondary organic aerosol formation in cloud droplets and aqueous particles (aqSOA): a review of laboratory, field and model studies, *Atmos. Chem. Phys.*, 11, 11069-11102, 10.5194/acp-11-11069-2011, 2011.
- Ervens, B.: Modeling the Processing of Aerosol and Trace Gases in Clouds and Fogs, *Chem Rev*, 115, 4157-4198, 10.1021/cr5005887, 2015.
- 865 Ervens, B., Sorooshian, A., Aldhaif, A. M., Shingler, T., Crosbie, E., Ziemba, L., Campuzano-Jost, P., Jimenez, J. L., and Wisthaler, A.: Is there an aerosol signature of chemical cloud processing?, *Atmos. Chem. Phys.*, 18, 16099-16119, 10.5194/acp-18-16099-2018, 2018.
- Fountoukis, C., and Nenes, A.: Continued development of a cloud droplet formation parameterization for global climate models, *Journal of Geophysical Research: Atmospheres*, 110, <https://doi.org/10.1029/2004JD005591>, 2005.
- 870 Gilardoni, S., Massoli, P., Paglione, M., Giulianelli, L., Carbone, C., Rinaldi, M., Decesari, S., Sandrini, S., Costabile, F., Gobbi, G. P., Pietrogrande, M. C., Visentin, M., Scotto, F., Fuzzi, S., and Facchini, M. C.: Direct observation of aqueous secondary organic aerosol from biomass-burning emissions, *Proceedings of the National Academy of Sciences*, 113, 10013-10018, 10.1073/pnas.1602212113, 2016.
- 875 Hakola, H., Hellén, H., Hemmilä, M., Rinne, J., and Kulmala, M.: In situ measurements of volatile organic compounds in a boreal forest, *Atmos. Chem. Phys.*, 12, 11665-11678, 10.5194/acp-12-11665-2012, 2012.
- Hari, P., and Kulmala, M.: Station for measuring ecosystem-atmosphere relations (SMEAR II), *Boreal Environmental Research*, 10, 315-322, 2005.
- 880 Harris, E., Sinha, B., van Pinxteren, D., Schneider, J., Poulain, L., Collett, J., D'Anna, B., Fahlbusch, B., Foley, S., Fomba, K. W., George, C., Gnauk, T., Henning, S., Lee, T., Mertes, S., Roth, A., Stratmann, F., Borrmann, S., Hoppe, P.,

- and Herrmann, H.: In-cloud sulfate addition to single particles resolved with sulfur isotope analysis during HCCT-2010, *Atmos. Chem. Phys.*, 14, 4219-4235, 10.5194/acp-14-4219-2014, 2014.
- Hartigan, J. A., and Wong, M. A.: Algorithm AS 136: A K-Means Clustering Algorithm, *Journal of the Royal Statistical Society. Series C (Applied Statistics)*, 28, 100-108, 10.2307/2346830, 1979.
- 885 Heikkinen, L., Äijälä, M., Riva, M., Luoma, K., Dällenbach, K., Aalto, J., Aalto, P., Aliaga, D., Aurela, M., Keskinen, H., Makkonen, U., Rantala, P., Kulmala, M., Petäjä, T., Worsnop, D., and Ehn, M.: Long-term sub-micrometer aerosol chemical composition in the boreal forest: inter- and intra-annual variability, *Atmos. Chem. Phys.*, 20, 3151-3180, 10.5194/acp-20-3151-2020, 2020.
- 890 Heikkinen, L., Äijälä, M., Daellenbach, K. R., Chen, G., Garmash, O., Aliaga, D., Graeffe, F., Rätty, M., Luoma, K., Aalto, P., Kulmala, M., Petäjä, T., Worsnop, D., and Ehn, M.: Eight years of sub-micrometre organic aerosol composition data from the boreal forest characterized using a machine-learning approach, *Atmos. Chem. Phys.*, 21, 10081-10109, 10.5194/acp-21-10081-2021, 2021.
- Helin, A., Niemi, J. V., Virkkula, A., Pirjola, L., Teinilä, K., Backman, J., Aurela, M., Saarikoski, S., Rönkkö, T., Asmi, E., and Timonen, H.: Characteristics and source apportionment of black carbon in the Helsinki metropolitan area, Finland, *Atmospheric Environment*, 190, 87-98, 10.1016/j.atmosenv.2018.07.022, 2018.
- 895 Häkkinen, S. A. K., Äijälä, M., Lehtipalo, K., Junninen, H., Backman, J., Virkkula, A., Nieminen, T., Vestenius, M., Hakola, H., Ehn, M., Worsnop, D. R., Kulmala, M., Petäjä, T., and Riipinen, I.: Long-term volatility measurements of submicron atmospheric aerosol in Hyytiälä, Finland, *Atmos. Chem. Phys.*, 12, 10771-10786, 10.5194/acp-12-10771-2012, 2012.
- 900 Junninen, H., Lauri, A., Keronen, P., Aalto, P., Hiltunen, V., Hari, P., and Kulmala, M.: Smart-SMEAR: online data exploration and visualization tool for SMEAR stations, *Boreal Environ Res*, 14, 447-457, 2009.
- Kaufman, L., and Rousseeuw, P. J.: Finding groups in data : an introduction to cluster analysis, *Wiley series in probability and mathematical statistics*, Wiley, New York, 342 pp., 1990.
- 905 Kesti, J., Asmi, E., O'Connor, E. J., Backman, J., Budhavant, K., Andersson, A., Dasari, S., Praveen, P. S., Zahid, H., and Gustafsson, Ö.: Changes in aerosol size distributions over the Indian Ocean during different meteorological conditions, *Tellus B: Chemical and Physical Meteorology*, 72, 1-14, 10.1080/16000889.2020.1792756, 2020.
- Kulmala, M., Rannik, U. I., Pirjola, L., Dal Maso, M., Karimäki, J., Asmi, A., Jäppinen, A., Karhu, V., Korhonen, H., Malvikko, S.-P., Raittila, J., Suni, T., Yli-Koivisto, S., and Vesala, T.: Characterization of atmospheric trace gas and aerosol concentrations at forest sites in southern and northern Finland using back trajectories, *Boreal environment research : an international interdisciplinary journal*, 315-336, 2000.
- 910 Laakso, L., Gronholm, T., Rannik, U., Kosmale, M., Fiedler, V., Vehkamäki, H., and Kulmala, M.: Ultrafine particle scavenging coefficients calculated from 6 years field measurements, *Atmospheric Environment*, 37, 3605-3613, 10.1016/S1352-2310(03)00326-1, 2003.
- 915 Lamkaddam, H., Dommen, J., Ranjithkumar, A., Gordon, H., Wehrle, G., Krechmer, J., Majluf, F., Salionov, D., Schmale, J., Bjelic, S., Carslaw, K. S., El Haddad, I., and Baltensperger, U.: Large contribution to secondary organic aerosol from isoprene cloud chemistry, *Science advances*, 7, 10.1126/sciadv.abe2952, 2021.
- Lei, T., Zuend, A., Cheng, Y., Su, H., Wang, W., and Ge, M.: Hygroscopicity of organic surrogate compounds from biomass burning and their effect on the efflorescence of ammonium sulfate in mixed aerosol particles, *Atmos. Chem. Phys.*, 18, 1045-1064, 10.5194/acp-18-1045-2018, 2018.
- 920 Leong, K. H., Beard, K. V., Stukel, J. J., and Hopke, P. K.: Factors Affecting the Collision of Aerosol-Particles with Small Water Drops, *Aerosol Sci Tech*, 2, 341-349, 1983.
- Liao, L., Dal Maso, M., Taipale, R., Rinne, J., Ehn, M., Junninen, H., Aijala, M., Nieminen, T., Alekseychik, P., Hulkkonen, M., Worsnop, D. R., Kerminen, V. M., and Kulmala, M.: Monoterpene pollution episodes in a forest environment: indication of anthropogenic origin and association with aerosol particles, *Boreal Environ Res*, 16, 288-303, 2011.
- 925 Liu, P. S. K., Deng, R., Smith, K. A., Williams, L. R., Jayne, J. T., Canagaratna, M. R., Moore, K., Onasch, T. B., Worsnop, D. R., and Deshler, T.: Transmission Efficiency of an Aerodynamic Focusing Lens System: Comparison of Model Calculations and Laboratory Measurements for the Aerodyne Aerosol Mass Spectrometer, *Aerosol Sci Tech*, 41, 721-733, 10.1080/02786820701422278, 2007.
- 930 Lowe, S. J., Partridge, D. G., Davies, J. F., Wilson, K. R., Topping, D., and Riipinen, I.: Key drivers of cloud response to surface-active organics, *Nature Communications*, 10, 5214, 10.1038/s41467-019-12982-0, 2019.

- Luoma, K., Virkkula, A., Aalto, P., Petäjä, T., and Kulmala, M.: Over a 10-year record of aerosol optical properties at SMEAR II, *Atmos. Chem. Phys.*, 19, 11363-11382, 10.5194/acp-19-11363-2019, 2019.
- Maechler, M., Rousseeuw, P., Struyf, A., Hubert, M., and Hornik, K.: *cluster: Cluster Analysis Basics and Extensions*. 2019.
- 935 Mandariya, A. K., Gupta, T., and Tripathi, S. N.: Effect of aqueous-phase processing on the formation and evolution of organic aerosol (OA) under different stages of fog life cycles, *Atmospheric Environment*, 206, 60-71, <https://doi.org/10.1016/j.atmosenv.2019.02.047>, 2019.
- Mann, H. B., and Whitney, D. R.: On a Test of Whether one of Two Random Variables is Stochastically Larger than the Other, *The Annals of Mathematical Statistics*, 18, 50-60, 11, 1947.
- 940 Mauritsen, T., Bader, J., Becker, T., Behrens, J., Bittner, M., Brokopf, R., Brovkin, V., Claussen, M., Crueger, T., Esch, M., Fast, I., Fiedler, S., Fläschner, D., Gayler, V., Giorgetta, M., Goll, D. S., Haak, H., Hagemann, S., Hedemann, C., Hohenegger, C., Ilyina, T., Jahns, T., Jimenez-de-la-Cuesta, D., Jungclaus, J., Kleinen, T., Kloster, S., Kracher, D., Kinne, S., Kleberg, D., Lasslop, G., Kornbluh, L., Marotzke, J., Matei, D., Meraner, K., Mikolajewicz, U., Modali, K., Möbis, B., Müller, W. A., Nabel, J. E. M. S., Nam, C. C. W., Notz, D., Nyawira, S.-S., Paulsen, H., Peters, K., Pincus, R., Pohlmann, H., Pongratz, J., Popp, M., Raddatz, T. J., Rast, S., Redler, R., Reick, C. H., Rohrschneider, T., Schemann, V., Schmidt, H., Schnur, R., Schulzweida, U., Six, K. D., Stein, L., Stemmler, I., Stevens, B., von Storch, J.-S., Tian, F., Voigt, A., Vrese, P., Wieners, K.-H., Wilkenskjaeld, S., Winkler, A., and Roeckner, E.: Developments in the MPI-M Earth System Model version 1.2 (MPI-ESM1.2) and Its Response to Increasing CO₂, *Journal of Advances in Modeling Earth Systems*, 11, 998-1038, <https://doi.org/10.1029/2018MS001400>, 2019.
- 945 McCulloch, C. E., Searle, S. R., and Neuhaus, J. M.: *Generalized, Linear, and Mixed Models*, 2nd ed., Wiley Series in Probability and Statistics, John Wiley & Sons, Inc., 424 pp., 2008.
- 950 McVay, R., and Ervens, B.: A microphysical parameterization of aqSOA and sulfate formation in clouds, *Geophysical Research Letters*, 44, 7500-7509, <https://doi.org/10.1002/2017GL074233>, 2017.
- Mehtätalo, L., and Lappi, J.: *Biometry for forestry and environmental data : with examples in R*, First edition. ed., Applied Environmental Series / Chapman & Hall/CRC, edited by: Lappi, J., CRC Press LLC, Boca Raton, FL, 2020.
- 955 Mikkonen, S., Korhonen, H., Romakkaniemi, S., Smith, J. N., Joutsensaari, J., Lehtinen, K. E. J., Hamed, A., Breider, T. J., Birmili, W., Spindler, G., Plass-Duelmer, C., Facchini, M. C., and Laaksonen, A.: Meteorological and trace gas factors affecting the number concentration of atmospheric Aitken (<i>D</i>_p = 50 nm) particles in the continental boundary layer: parameterization using a multivariate mixed effects model, *Geosci. Model Dev.*, 4, 1-13, 10.5194/gmd-4-1-2011, 2011.
- 960 Nenes, A., and Seinfeld, J. H.: Parameterization of cloud droplet formation in global climate models, *Journal of Geophysical Research: Atmospheres*, 108, <https://doi.org/10.1029/2002JD002911>, 2003.
- Ng, N. L., Herndon, S. C., Trimborn, A., Canagaratna, M. R., Croteau, P. L., Onasch, T. B., Sueper, D., Worsnop, D. R., Zhang, Q., Sun, Y. L., and Jayne, J. T.: An Aerosol Chemical Speciation Monitor (ACSM) for Routine Monitoring of the Composition and Mass Concentrations of Ambient Aerosol, *Aerosol Sci Tech*, 45, 780-794, 10.1080/02786826.2011.560211, 2011.
- 965 Nicholson, K. W., Branson, J. R., and Giess, P.: Field-Measurements of the Below-Cloud Scavenging of Particulate Material, *Atmos Environ a-Gen*, 25, 771-777, 10.1016/0960-1686(91)90075-I, 1991.
- Ohata, S., Moteki, N., Mori, T., Koike, M., and Kondo, Y.: A key process controlling the wet removal of aerosols: new observational evidence, *Scientific Reports*, 6, 34113, 10.1038/srep34113, 2016.
- 970 Pajunoja, A., Lambe, A. T., Hakala, J., Rastak, N., Cummings, M. J., Brogan, J. F., Hao, L., Paramonov, M., Hong, J., Prisle, N. L., Malila, J., Romakkaniemi, S., Lehtinen, K. E. J., Laaksonen, A., Kulmala, M., Massoli, P., Onasch, T. B., Donahue, N. M., Riipinen, I., Davidovits, P., Worsnop, D. R., Petäjä, T., and Virtanen, A.: Adsorptive uptake of water by semisolid secondary organic aerosols, *Geophysical Research Letters*, 42, 3063-3068, <https://doi.org/10.1002/2015GL063142>, 2015.
- 975 Paramonov, M., Gronholm, T., and Virkkula, A.: Below-cloud scavenging of aerosol particles by snow at an urban site in Finland, *Boreal Environ Res*, 16, 304-320, 2011.
- Partridge, D. G., Vrugt, J. A., Tunved, P., Ekman, A. M. L., Struthers, H., and Sorooshian, A.: Inverse modelling of cloud-aerosol interactions – Part 2: Sensitivity tests on liquid phase clouds using a Markov chain Monte Carlo based simulation approach, *Atmos. Chem. Phys.*, 12, 2823-2847, 10.5194/acp-12-2823-2012, 2012.

- 980 Patokoski, J., Ruuskanen, T. M., Kajos, M. K., Taipale, R., Rantala, P., Aalto, J., Ryyppö, T., Nieminen, T., Hakola, H., and Rinne, J.: Sources of long-lived atmospheric VOCs at the rural boreal forest site, SMEAR II, *Atmos. Chem. Phys.*, 15, 13413-13432, 10.5194/acp-15-13413-2015, 2015.
- Paulot, F., Fan, S., and Horowitz, L. W.: Contrasting seasonal responses of sulfate aerosols to declining SO₂ emissions in the Eastern U.S.: Implications for the efficacy of SO₂ emission controls, *Geophysical Research Letters*, 44, 455-464, <https://doi.org/10.1002/2016GL070695>, 2017.
- 985 Petzold, A., Ogren, J. A., Fiebig, M., Laj, P., Li, S. M., Baltensperger, U., Holzer-Popp, T., Kinne, S., Pappalardo, G., Sugimoto, N., Wehrli, C., Wiedensohler, A., and Zhang, X. Y.: Recommendations for reporting "black carbon" measurements, *Atmos. Chem. Phys.*, 13, 8365-8379, 10.5194/acp-13-8365-2013, 2013.
- R Core Team: R: A language and environment for statistical computing. In: R Foundation for Statistical Computing, Vienna, Austria, 2019.
- 990 Riuttanen, L., Hulkkonen, M., Dal Maso, M., Junninen, H., and Kulmala, M.: Trajectory analysis of atmospheric transport of fine particles, SO₂, NO_x and O₃ to the SMEAR II station in Finland in 1996–2008, *Atmos. Chem. Phys.*, 13, 2153-2164, 10.5194/acp-13-2153-2013, 2013.
- Singh, A., Rajput, P., Sharma, D., Sarin, M. M., and Singh, D.: Black Carbon and Elemental Carbon from Postharvest Agricultural-Waste Burning Emissions in the Indo-Gangetic Plain, *Adv Meteorol*, 2014, Artn 179301, 10.1155/2014/179301, 2014.
- 995 Slinn, W. G. N.: Precipitation Scavenging, *Atmospheric Sciences and Power Production*, Chapter 11, Division of Biomedical Environmental Research, U.S. Department of Energy, Washington, D.C., 1983.
- Sogacheva, L., Dal Maso, M., Kerminen, V. M., and Kulmala, M.: Probability of nucleation events and aerosol particle concentration in different air mass types arriving at Hyytiälä southern Finland, based on back trajectories analysis, *Boreal Environ Res*, 10, 479-491, 2005.
- 1000 Sorooshian, A., Varutbangkul, V., Brechtel, F. J., Ervens, B., Feingold, G., Bahreini, R., Murphy, S. M., Holloway, J. S., Atlas, E. L., Buzorius, G., Jonsson, H., Flagan, R. C., and Seinfeld, J. H.: Oxalic acid in clear and cloudy atmospheres: Analysis of data from International Consortium for Atmospheric Research on Transport and Transformation 2004, *Journal of Geophysical Research: Atmospheres*, 111, <https://doi.org/10.1029/2005JD006880>, 2006.
- 1005 Sorooshian, A., Lu, M.-L., Brechtel, F. J., Jonsson, H., Feingold, G., Flagan, R. C., and Seinfeld, J. H.: On the Source of Organic Acid Aerosol Layers above Clouds, *Environ Sci Technol*, 41, 4647-4654, 10.1021/es0630442, 2007.
- Official Statistics of Finland (OSF): Population structure: http://www.stat.fi/til/vaerak/index_en.html, 2019.
- 1010 Stein, A. F., Draxler, R. R., Rolph, G. D., Stunder, B. J. B., Cohen, M. D., and Ngan, F.: NOAA's Hysplit Atmospheric Transport and Dispersion Modeling System, *B Am Meteorol Soc*, 96, 2059-2077, 10.1175/Bams-D-14-00110.1, 2015.
- Textor, C., Schulz, M., Guibert, S., Kinne, S., Balkanski, Y., Bauer, S., Berntsen, T., Berglen, T., Boucher, O., Chin, M., Dentener, F., Diehl, T., Easter, R., Feichter, H., Fillmore, D., Ghan, S., Ginoux, P., Gong, S., Kristjansson, J. E., Krol, M., Lauer, A., Lamarque, J. F., Liu, X., Montanaro, V., Myhre, G., Penner, J., Pitari, G., Reddy, S., Seland, O., Stier, P., Takemura, T., and Tie, X.: Analysis and quantification of the diversities of aerosol life cycles within AeroCom, *Atmos Chem Phys*, 6, 1777-1813, 10.5194/acp-6-1777-2006, 2006.
- 1015 Tiedtke, M.: Representation of Clouds in Large-Scale Models, *Mon Weather Rev*, 121, 3040-3061, 10.1175/1520-0493(1993)121<3040:Rocils>2.0.Co;2, 1993.
- 1020 Tunved, P., Ström, J., and Hansson, H. C.: An investigation of processes controlling the evolution of the boundary layer aerosol size distribution properties at the Swedish background station Aspvreten, *Atmos. Chem. Phys.*, 4, 2581-2592, 10.5194/acp-4-2581-2004, 2004.
- Tunved, P., Ström, J., and Krejci, R.: Arctic aerosol life cycle: linking aerosol size distributions observed between 2000 and 2010 with air mass transport and precipitation at Zeppelin station, Ny-Ålesund, Svalbard, *Atmos. Chem. Phys.*, 13, 3643-3660, 10.5194/acp-13-3643-2013, 2013.
- 1025 Virkkula, A., Mäkelä, T., Hillamo, R., Yli-Tuomi, T., Hirsikko, A., Hämeri, K., and Koponen, I. K.: A Simple Procedure for Correcting Loading Effects of Aethalometer Data, *Journal of the Air & Waste Management Association*, 57, 1214-1222, 10.3155/1047-3289.57.10.1214, 2007.

- 1030 Väisänen, O., Ruuskanen, A., Ylissirniö, A., Miettinen, P., Portin, H., Hao, L., Leskinen, A., Komppula, M., Romakkaniemi, S., Lehtinen, K. E. J., and Virtanen, A.: In-cloud measurements highlight the role of aerosol hygroscopicity in cloud droplet formation, *Atmos. Chem. Phys.*, 16, 10385-10398, 10.5194/acp-16-10385-2016, 2016.
- Wang, X., Zhang, L., and Moran, M. D.: Uncertainty assessment of current size-resolved parameterizations for below-cloud particle scavenging by rain, *Atmos. Chem. Phys.*, 10, 5685-5705, 10.5194/acp-10-5685-2010, 2010.
- 1035 Wang, Y., Xia, W., and Zhang, G. J.: What rainfall rates are most important to wet removal of different aerosol types?, *Atmos. Chem. Phys.*, 21, 16797-16816, 10.5194/acp-21-16797-2021, 2021.
- Wonaschuetz, A., Sorooshian, A., Ervens, B., Chuang, P. Y., Feingold, G., Murphy, S. M., de Gouw, J., Warneke, C., and Jonsson, H. H.: Aerosol and gas re-distribution by shallow cumulus clouds: An investigation using airborne measurements, *Journal of Geophysical Research: Atmospheres*, 117, <https://doi.org/10.1029/2012JD018089>, 2012.
- 1040 Wu, Z. J., Poulain, L., Henning, S., Dieckmann, K., Birmili, W., Merkel, M., van Pinxteren, D., Spindler, G., Müller, K., Stratmann, F., Herrmann, H., and Wiedensohler, A.: Relating particle hygroscopicity and CCN activity to chemical composition during the HCCT-2010 field campaign, *Atmos. Chem. Phys.*, 13, 7983-7996, 10.5194/acp-13-7983-2013, 2013.
- Xie, Y., Ding, A., Nie, W., Mao, H., Qi, X., Huang, X., Xu, Z., Kerminen, V.-M., Petäjä, T., Chi, X., Virkkula, A., Boy, M., Xue, L., Guo, J., Sun, J., Yang, X., Kulmala, M., and Fu, C.: Enhanced sulfate formation by nitrogen dioxide: Implications from in situ observations at the SORPES station, *Journal of Geophysical Research: Atmospheres*, 120, 12679-12694, <https://doi.org/10.1002/2015JD023607>, 2015.
- 1045 Xu, W., Ovadnevaite, J., Fossun, K. N., Lin, C., Huang, R. J., O'Dowd, C., and Ceburnis, D.: Aerosol hygroscopicity and its link to chemical composition in the coastal atmosphere of Mace Head: marine and continental air masses, *Atmos. Chem. Phys.*, 20, 3777-3791, 10.5194/acp-20-3777-2020, 2020.
- 1050 Xue, J., Yuan, Z., Griffith, S. M., Yu, X., Lau, A. K. H., and Yu, J. Z.: Sulfate Formation Enhanced by a Cocktail of High NO_x, SO₂, Particulate Matter, and Droplet pH during Haze-Fog Events in Megacities in China: An Observation-Based Modeling Investigation, *Environ Sci Technol*, 50, 7325-7334, 10.1021/acs.est.6b00768, 2016.
- Yli-Juuti, T., Mielonen, T., Heikkinen, L., Arola, A., Ehn, M., Isokääntä, S., Keskinen, H.-M., Kulmala, M., Laakso, A., Lipponen, A., Luoma, K., Mikkonen, S., Nieminen, T., Paasonen, P., Petäjä, T., Romakkaniemi, S., Tonttila, J., Kokkola, H., and Virtanen, A.: Significance of the organic aerosol driven climate feedback in the boreal area, *Nature Communications*, 12, 5637, 10.1038/s41467-021-25850-7, 2021.
- 1055 Zhang, Z., and Chen, Q.: Comparison of the Eulerian and Lagrangian methods for predicting particle transport in enclosed spaces, *Atmospheric Environment*, 41, 5236-5248, <https://doi.org/10.1016/j.atmosenv.2006.05.086>, 2007.
- 1060 Zieger, P., Väisänen, O., Corbin, J. C., Partridge, D. G., Bastelberger, S., Mousavi-Fard, M., Rosati, B., Gysel, M., Krieger, U. K., Leck, C., Nenes, A., Riipinen, I., Virtanen, A., and Salter, M. E.: Revising the hygroscopicity of inorganic sea salt particles, *Nature Communications*, 8, 15883, 10.1038/ncomms15883, 2017.